Bonding and Substituent Effects in Electron-Rich Mononuclear Ruthenium σ-Arylacetylides of the Formula $[(\eta^2\text{-dppe})(\eta^5\text{-}C_5Me_5)Ru(C{\equiv}C)\text{-}1,4\text{-}(C_6H_4)X][PF_6]_n$ (n = 0, 1; X = NO_2, CN, F, H, OMe, NH_2)

Frédéric Paul,*[,†] Benjamin G. Ellis,[†,‡] Michael I. Bruce,*[,‡] Loic Toupet,[§] Thierry Roisnel,[||] Karine Costuas,[||] Jean-François Halet,[||] and Claude Lapinte[†]

Organométalliques et Catalyse: Chimie et Electrochimie Moléculaires, UMR CNRS 6509, Institut de Chimie, Université de Rennes 1, Campus de Beaulieu, 35042 Rennes Cedex, France, Department of Chemistry, University of Adelaide, South Australia 5005, Australia, Groupe Matière Condensée et Matériaux, UMR CNRS 6626, Université de Rennes 1, Campus de Beaulieu, 35042 Rennes Cedex, France, and Laboratoire de Chimie du Solide et Inorganique Moléculaire, UMR CNRS 6511, Institut de Chimie, Université de Rennes 1, Campus de Beaulieu, 35042 Rennes Cedex, France

Received September 16, 2005

This study reports the isolation and the structural (X-ray), UV−vis, and NMR characterization of a series of electron-rich Ru(II) acetylide complexes of the formula (η^2-dppe)(η^5-C_5Me_5)Ru(C≡C)-1,4-(C_6H_4)X (**1a**−**f**; X = NO_2, CN, F, H, OMe, NH_2) and (η^2-dppe)(η^5-C_5Me_5)Ru(C≡C)-1,3-(C_6H_4)F (**1c**-*m*), as well as the spectroscopic (near-IR and ESR) in situ characterization of the corresponding elusive Ru(III) radical cations. The spectroscopic data are discussed in connection with DFT computations, and a consistent picture of the electronic structure of these Ru(II) and Ru(III) acetylide complexes is proposed. Notably, the strong reactivity of the Ru(III) radicals evidenced in this contribution constitutes a major difference with the relative stability of the known iron analogues.

Introduction

Over the last few years, electron-rich mono- or polynuclear metal acetylides have attracted particular attention for the realization of molecular devices.[1] These organometallic fragments have shown interesting properties when used as electroactive end groups in conjunction with various unsaturated bridges.[2−7] Depending on the nature of the metal, on the structure and connectivity of the central spacer, and on the redox state of the compound, molecular wires exhibiting quite different magnetic, optic, or electronic properties have been synthesized.[2b,3b−d,5,7−11] Alternatively, several electron-rich group VIII metal−acetylide complexes have recently been demonstrated to constitute very interesting functional groups for redox switching of a given molecular property.[1a,e,12−13] Central to their use in such applications is the question of electronic com-

* To whom correspondence should be addressed. Fax: (33) 2 23 23 56 37 (F.P.); (61) 8 8303 4358 (M.I.B.). E-mail: frederic.paul@univ-rennes1.fr (F.P.); michael.bruce@adelaide.edu.au (M.I.B.).

† UMR CNRS 6509, Université de Rennes 1.

‡ University of Adelaide.

§ UMR CNRS 6626, Université de Rennes 1.

|| UMR CNRS 6511, Université de Rennes 1.

(1) See for instance: (a) Cifuentes, M. P.; Humphrey, M. G.; Morall, J. P.; Samoc, M.; Paul, F.; Roisnel, T.; Lapinte, C. *Organometallics* **2005**, *24*, 4280−4288. (b) Blum, A. S.; Ren, T.; Parish, D. A.; Trammell, S. A.; Moore, M. H.; Kushmerick, J. G.; Xu, G.-L.; Deschamps, J. R.; Polack, S. K.; Shashidar, R. *J. Am. Chem. Soc.* **2005**, *127*, 10010−10011. (c) Fillaut, J.-L.; Perruchon, J.; Blanchard, P.; Roncali, J.; Gohlen, S.; Allain, M.; Migalska-Zalas, A.; Kityk, I. V.; Sahraoui, B. *Organometallics* **2005**, *24*, 687−695. (d) Qi, H.; Sharma, S.; Li, Z.; Snider, G. L.; Orlov, A. O.; Lent, S. S.; Fehlner, T. P. *J. Am. Chem. Soc.* **2003**, *125*, 15250−15259. (e) Wong, K. M.-C.; Lam, S. C.-F.; Ko, C.-C.; Zhu, N.; Yam, V. W.-W.; Roué, S.; Lapinte, C.; Fathallah, S.; Costuas, K.; Kahlal, S.; Halet, J.-F. *Inorg. Chem.* **2003**, *42*, 7086−7097. (f) Powell, C. E.; Humphrey, M. G. *Coord. Chem. Rev.* **2004**, *248*, 725−756. (g) Hu, Q. Y.; Lu, W. X.; Tang, H. D.; Sung, H. H. Y.; Wen, T. B.; Williams, I. D.; Wong, G. K. L.; Lin, Z.; Jia, G. *Organometallics* **2005**, *24*, 3966−3973.

(2) (a) Rigaut, S.; Touchard, D.; Dixneuf, P. H. *Coord. Chem. Rev.* **2004**, *248*, 1585−1601. (b) Rigaut, S.; Perruchon, J.; Le Pichon, L.; Touchard, D.; Dixneuf, P. H. *J. Organomet. Chem.* **2003**, *670*, 37−44. (c) Wong, C.-Y.; Che, C.-M.; Chan, M. C. W.; Han, J.; Leung, K.-H.; Phillips, D. L.; Wong, K.-Y.; Zhu, N. *J. Am. Chem. Soc.* **2005**, 127, 13997−14007.

(3) (a) Venkatesan, K.; Fox, T.; Schmalle, H. W.; Berke, H. *Organometallics* **2005**, *24*, 2834−2847. (b) Venkatesan, K.; Blacque, O.; Fox, T.; Alfonso, M.; Schmalle, H. W.; Berke, H. *Organometallics* **2004**, *23*, 1183−1186. (c) Fernandez, F. J.; Venkatesan, K.; Blacque, O.; Alfonso, M.; Schmalle, H.; Berke, H. *Chem. Eur. J.* **2003**, *9*, 6192−6209. (d) Venkatesan, K.; Fernandez, F. J.; Blacque, O.; Fox, T.; Alfonso, M.; Schmalle, H. W.; Berke, H. *Chem. Commun.* **2003**, 2006−2008. (e) Kheradmandan, S.; Heinze, K.; Schmalle, H.; Berke, H. *Angew. Chem., Int. Ed. Engl.* **1999**, *38*, 2270−2273.

(4) Yam, V. W.-W. *Acc. Chem. Res.* **2002**, *35*, 555−563.

(5) (a) Whittall, I. R.; McDonagh, A. M.; Humphrey, M. G.; Samoc, M. *Adv. Organomet. Chem.* **1998**, *42*, 291−362. (b) Whittall, I. R.; McDonagh, A. M.; Humphrey, M. G.; Samoc, M. *Adv. Organomet. Chem.* **1998**, *43*, 349−405.

(6) (a) Weyland, T.; Ledoux, I.; Brasselet, S.; Zyss, J.; Lapinte, C. *Organometallics* **2000**, *19*, 5235−5237. (b) Weyland, T.; Costuas, K.; Toupet, L.; Halet, J.-F.; Lapinte, C. *Organometallics* **2000**, *19*, 4228−4239. (c) Weyland, T.; Costuas, K.; Mari, A.; Halet, J.-F.; Lapinte, C. *Organometallics* **1998**, *17*, 5569−5579. (d) Weyland, T.; Lapinte, C.; Frapper, G.; Calhorda, M. J.; Halet, J.-F.; Toupet, L. *Organometallics* **1997**, *16*, 2024−2031.

(7) (a) Bruce, M. I. *Coord. Chem. Rev.* **1997**, *166*, 91−119. (b) Bruce, M. I. *Chem. Rev.* **1998**, *98*, 2797−2858. (c) Bruce, M. I.; Low, P. J. *Adv. Organomet. Chem.* **2004**, *50*, 179−444.

(8) Szafert, S.; Gladysz, J. A. *Chem. Rev.* **2003**, *103*, 4175−4205.

(9) (a) Paul, F.; Lapinte, C. In *Unusual Structures and Physical Properties in Organometallic Chemistry*; Gielen, M., Willem, R., Wrackmeyer, B., Eds.; Wiley: San Francisco, 2002; pp 219−295. (b) Paul, F.; Lapinte, C. *Coord. Chem. Rev.* **1998**, *178/180*, 427−505.

(10) (a) Roué, S.; Le Stang, S.; Toupet, L.; Lapinte, C. *C. R. Chim.* **2003**, *6*, 353−366. (b) Le Narvor, N.; Toupet, L.; Lapinte, C. *J. Am. Chem. Soc.* **1995**, *117*, 7129−7138. (c) Le Narvor, N.; Lapinte, C. *C. R. Acad. Sci., Ser. IIc: Chim.* **1998**, 745−749. (d) Coat, F.; Lapinte, C. *Organometallics* **1996**, *15*, 476−479. (e) Coat, F.; Paul, F.; Lapinte, C.; Toupet, L.; Costuas, K.; Halet, J.-F. *J. Organomet. Chem.* **2003**, *683*, 368−378.

(11) Ren, T. *Organometallics* **2005**, *24*, 4854−4870 and references cited therein.

10.1021/om050799t CCC: $33.50
Publication on Web 12/27/2005

Chart 1

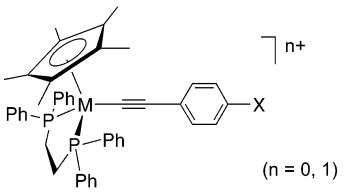

X	M = Ru	M = Fe
	1a: NO_2	**2a**: NO_2
	1b: CN	**2b**: CN
	1c: F	**2c**: F
	1d: H	**2d**: H
	1e: OMe	**2e**: OMe
	1f: NH_2	**2f**: NH_2

munication between the metal and the rest of the molecule via the alkynyl bridge.[14,15] In this respect, and following the recent synthesis of polynuclear architectures bearing "(η^2-dppe)(η^5-C_5Me_5)Ru(C≡C)−" electroactive end groups,[16] we were interested in comparing the electronic substituent effects in a series of mononuclear model complexes of the formula [(η^2-dppe)(η^5-C_5Me_5)Ru(C≡C)-1,4-(C_6H_4)X][PF_6]$_n$ (n = 0, 1; **1a**−**f**/**1a**−**f**$^+$) (Chart 1) with those operative in the series of iron analogues [(η^2-dppe)(η^5-C_5Me_5)Fe(C≡C)-1,4-(C_6H_4)X][PF_6]$_n$ (n = 0, 1; **2a**−**f**/**2a**−**f**$^+$), previously investigated by some of us.[12,17] Given the significantly larger electronegativity of ruthenium relative to iron, we anticipated that the bonding and the properties in each redox state might be somewhat different, as observed for the dinuclear butadiynediyl complexes.[16a] For instance, in line with previous hyperpolarizability measurements,[12] a smaller degree of back-donation from filled d metal-based (M = Ru, Fe) molecular orbitals (MOs) into the empty alkynyl π* MOs was expected in the Ru(II) case.[18]

We therefore report in the following (i) the synthesis and characterization of several such Ru(II) complexes (**1a**−**f**), (ii) the in situ characterization of the corresponding Ru(III) parents generated after chemical oxidation (**1a**−**f**$^+$), (iii) DFT computations on several Ru(II) and Ru(III) representatives, and (iv) correlations of selected data with electronic substituent parameters (ESP). The bonding within the "Ru−C≡C-1,4-C_6H_4−" core is then discussed along with the X-substituent electronic effects and subsequently compared to results previously obtained with the known iron analogues (**2a**−**f**/**2a**−**f**$^+$).[17c] This work actually reveals several notable differences between these series of isoelectronic and isolobal complexes.

Results

Synthesis and Characterization of the Ru(II) Complexes. Many of the complexes were obtained by the traditional route developed by Bruce et al. for Ru complexes: i.e., activation of the preformed functional arylacetylide starting from the known chloride precursor (η^2-dppe)(η^5-C_5Me_5)RuCl (**3**).[16c,19] This synthetic approach is quite versatile and allows for the isolation of most compounds in a straightforward way (Scheme 1).[20] As shown in the case of $Me_3SiC{\equiv}CC_6H_4NO_2$-4, prior deprotection of the silyl group of the phenylalkyne is not necessary, since it occurs spontaneously during the course of the reaction. The vinylidene complexes formed as intermediates were not isolated but deprotonated in situ using ^{t}BuOK to yield several of the desired acetylide complexes (**1a**,**c**−**f**). The quantitative formation of the vinylidene salts was checked by ^{1}H and ^{31}P NMR each time.

In the case of the cyano and fluoride substituents, the previous reaction did not work properly. Small amounts of unidentified compounds were always isolated with the desired acetylide complex during the workup, and conversion of the starting chloro complex **3** was uncomplete. We therefore devised another way to access the Ru(II) acetylides with these particular substituents and found it more convenient to use a Sonogashira-type catalytic coupling procedure with the terminal acetylide complex (η^2-dppe)(η^5-C_5Me_5)RuC≡CH (**4**). Such a procedure, starting from electron-rich metalated alkynes such as **4**, has already been proven to be quite versatile[21−24] and presently allowed the isolation of the target complexes **1b** (X = CN) and **1c** (X = F) and also of the meta isomer of **1c** (**1c**-*m*) with good yields (Scheme 2). By this route, **1a** was isolated with a lower yield (see Experimental Section) than by the previous one (Scheme 1). However, with this particular substituent, it is the separation of **1a** from excess $BrC_6H_4NO_2$-4 which proves detrimental to the final yield, since NMR reveals that **1a** is quantitatively formed by the reaction given in Scheme 2. For other substituents, the crude samples of the Ru(II) complexes isolated by extraction right after the reaction are usually fairly clean. The compounds can then be further purified by flash chromatography on alumina, before being crystallized from solvent mixtures.

Unambiguous solid-state characterization of each of the Ru(II) acetylide complexes (**1a**−**f**) was carried out by a single-crystal X-ray structural determination. In addition, correct elemental analyses and LSI-MS were obtained. Notably, during LSI-MS characterization, quite intense peaks corresponding to the carbonyl ruthenium (**5**$^+$) adduct were detected (Chart 2), while such complexes were always absent from the original samples.[25,26] An analogous Fe(II) cation was also often detected by MS when **2a**−**f** were subjected to LSI-MS analysis.

(12) Paul, F.; Costuas, K.; Ledoux, I.; Deveau, S.; Zyss, J.; Halet, J.-F.; Lapinte, C. *Organometallics* **2002**, *21*, 5229−5235.

(13) (a) Powell, C. E.; Cifuentes, M. P.; Morall, J. P.; Stranger, R.; Humphrey, M. G.; Samoc, M.; Luther-Davies, B.; Heath, G. A. *J. Am. Chem. Soc.* **2003**, *125*, 602−610. (b) Powell, C. E.; Humphrey, M. G.; Cifuentes, M. P.; Morall, J. P.; Samoc, M.; Luther-Davies, B. *J. Phys. Chem. A* **2003**, *107*, 11264−11266. (c) Cifuentes, M. P.; Powell, C. E.; Humphrey, M. G.; Heath, G. A.; Samoc, M.; Luther-Davies, B. *J. Phys. Chem. A* **2001**, *105*, 9625−9627.

(14) Manna, J.; John, K. D.; Hopkins, M. D. *Adv. Organomet. Chem.* **1995**, *38*, 80−154.

(15) (a) Lichtenberger, D. L.; Renshaw, S. K. *Organometallics* **1993**, *12*, 3522−3526. (b) Lichtenberger, D. L.; Renshaw, S. K.; Bullock, R. M. *J. Am. Chem. Soc.* **1993**, *115*, 3276−3285. (c) Lichtenberger, D. L.; Gruhn, N. E.; Renshaw, S. K. *J. Mol. Struct.* **1997**, *405*, 79−86.

(16) (a) Bruce, M. I.; Costuas, K.; Davin, T.; Ellis, B. G.; Halet, J.-F.; Lapinte, C.; Low, P. J.; Smith, M. E.; Skelton, B. W.; Toupet, L.; White, A. H. *Organometallics* **2005**, *24*, 3864−3881. (b) Bruce, M. I.; Ellis, B. G.; Low, P. J.; Skelton, B. W.; White, A. H. *Organometallics* **2003**, *22*, 3184−3198. (c) Bruce, M. I.; Skelton, B. W.; White, A. H.; Zaitseva, N. N. *J. Organomet. Chem.* **2002**, *650*, 141−150.

(17) (a) Denis, R.; Toupet, L.; Paul, F.; Lapinte, C. *Organometallics* **2000**, *19*, 4240−4251. (b) Paul, F.; Mevellec, J.-Y.; Lapinte, C. *Dalton Trans.* **2002**, 1783−1790. (c) Costuas, K.; Paul, F.; Toupet, L.; Halet, J.-F.; Lapinte, C. *Organometallics* **2004**, *23*, 2053−2068. (d) Paul, F.; Toupet, L.; Thépot, J.-Y.; Costuas, K.; Halet, J.-F.; Lapinte, C. *Organometallics* **2005**, *24*, 5464−5478.

(18) Delfs, C. D.; Stranger, R.; Humphrey, M. G.; MacDonagh, A. M. *J. Organomet. Chem.* **2000**, *607*, 208−212.

(19) Bruce, M. I.; Wallis, R. C. *J. Organomet. Chem.* **1978**, *161*, C1−C4.

(20) Bitcon, C.; Whiteley, M. W. *J. Organomet. Chem.* **1987**, *336*, 385−392.

(21) (a) Bruce, M. I.; Ke, M.; Low, P. J. *J. Chem. Soc., Chem. Commun.* **1996**, 2405−2406. (b) Bruce, M. I.; Ke, M.; Low, P. J.; Skelton, B. W.; White, A. H. *Organometallics* **1998**, *17*, 3539−3549.

(22) Denis, R.; Weyland, T.; Paul, F.; Lapinte, C. *J. Organomet. Chem.* **1997**, *545/546*, 615−618.

(23) Hurst, S. K.; Cifuentes, M. P.; MacDonagh, A. M.; Humphrey, M. G.; Samoc, M.; Luther-Davies, B.; Asselberghs, I.; Persoons, A. *J. Organomet. Chem.* **2002**, *642*, 259−267.

(24) Courmarcel, J.; Le Gland, G.; Toupet, L.; Paul, F.; Lapinte, C. *J. Organomet. Chem.* **2003**, *670*, 108−122.

(25) This known compound presents a characteristic[27] and intense infrared absorption (ν_{CO} at 1972 cm^{-1}) and a ^{31}P shift around 72 ppm.[26]

(26) Bruce, M. I.; Ellis, B. G.; Skelton, B. W.; White, A. H. *J. Organomet. Chem.* **2005**, *690*, 792−801.

Scheme 1

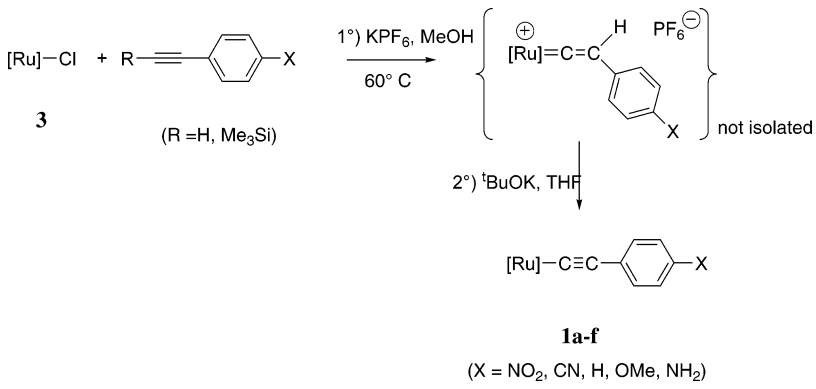

Scheme 2

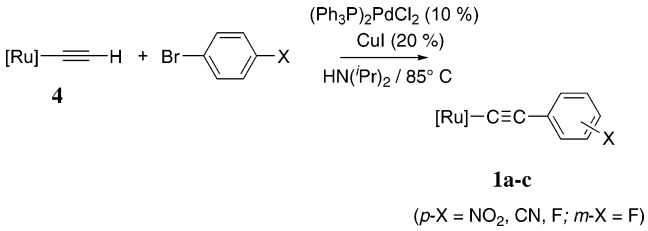

Chart 2

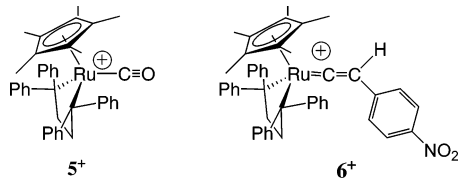

Table 1. Infrared Data for $[(\eta^2\text{-dppe})(\eta^5\text{-}C_5Me_5)Ru(C{\equiv}C\text{-}C_6H_4X)]^{0/+}$ Complexes in CH_2Cl_2 Solution (cm^{-1})

	$\nu_{C\equiv C}$		
X	Ru(II)[a]	Ru(III)	$\Delta\nu_{C\equiv C}$[b]
4-NO_2 (**1a**)	2048	1942	−90[d]
	2017		
4-CN (**1b**)[c]	2060	1944	−105[d]
	2039		
3-F (**1c-*m***)	2072	nd[e]	/
	2058		
4-F (**1c**)	2072	1930	−142
4-H (**1d**)	2071	1930[f]	−141
4-OMe (**1e**)	2074	1929	−145
4-NH_2 (**1f**)	2075	1940[f]	−135[d]
	2050 (sh)		

[a] Solid-state $\nu_{C\equiv C}$ values obtained in KBr for isolated complexes are given in the Experimental Section. [b] Neutral vs oxidized $\nu_{C\equiv C}$ difference. [c] For this complex, the $\nu_{C\equiv N}$ value is shifted from 2218 cm^{-1} to 2227 cm^{-1}. [d] Mean $\Delta\nu_{C\equiv C}$ value. [e] Not determined. [f] Tentative assignment.

These carbonyl complexes are probably formed in situ, by reaction of the M(II) acetylide complexes (M = Ru, Fe) with traces of molecular oxygen[28] or water, either before or after ionization/protonation[29] by the matrix.

The acetylide complexes **1a**−**f** were also characterized by the usual spectroscopic methods. NMR, infrared (Table 1), and Raman spectra contained the spectral signatures expected for these compounds. Thus, a single peak is observed by $^{31}P\{^1H\}$ NMR near 82 ppm for the two equivalent phosphorus atoms in solution and a triplet with a coupling constant of ca. 25 Hz, characteristic of the α-acetylide carbon atom, can be identified in the ^{13}C NMR spectrum in each case (see Experimental Section).[26] For all complexes, a strong $\nu(C{\equiv}C)$ band near 2050 cm^{-1} is also apparent in solution and in the solid state, which can be detected by either infrared or Raman spectroscopy. In solution, this absorption is split respectively by 31 and 21 cm^{-1} for the nitro- and cyano-containing complexes (**1a**,**b**), presumably by reason of Fermi coupling.[17b]

Table 2. UV−vis Data for $(\eta^2\text{-dppe})(\eta^5\text{-}C_5Me_5)Ru(C{\equiv}C\text{-}C_6H_4X)$ Complexes in CH_2Cl_2

X	abs, nm ($10^{-3}\epsilon$, M^{-1} cm^{-1})
4-NO_2 (**1a**)	264 (113.2); 322 (sh, 10.1); 500 (18.9)
4-CN (**1b**)	250 (sh, 23.1); 338 (sh, 9.3); 384 (19.2)
3-F (**1c**)	328 (17.9)
4-F (**1c-*m***)	248 (sh, 26.0); 306 (19.0)
4-H (**1d**)	252 (sh, 24.5); 318 (21.1)
4-OMe (**1e**)	252 (sh, 37.2); 300 (21.4)
4-NH_2 (**1f**)	254 (sh, 25.4); 304 (23.2)

For all compounds a rather intense electronic transition is observed in the 300−500 nm range, which explains the purple (**1a**) or orange-yellow (**1b**−**f**) color of the complexes (Table 2).[12] We attribute this electronic transition to an MLCT process by analogy with **2a**−**f**.[17c,30] This electronic transition is ipsochromically shifted by electron-releasing substituents, a substituent effect which also would be in accordance with an MLCT process.[17c] For all complexes, more intense absorptions, possibly corresponding to ligand-based $\pi-\pi^*$ or $n-\pi^*$ transitions, are also observed above 250 nm, while for the nitro complex **1a**, an additional weak transition is detected near 320 nm. We tentatively attribute this to a nitro-based $n-\pi^*$ transition.[17a]

Cyclic voltammograms (CVs) of all Ru(II) complexes were recorded between 1.0 and −1.5 V vs the standard calomel electrode (SCE). All complexes display an apparently reversible or quasi-reversible (in the chemical sense) one-electron wave (Table 3) in the range 0.05−0.40 V, corresponding to the metal-centered Ru(II)/Ru(III) oxidation. As expected, electron-releasing substituents facilitate this process, shifting the redox potential toward more negative values from ca. 350 mV on going from the nitro (**1a**) to the amino complex (**1f**) (Figure 1a). For **1a**, an additional nonreversible process is observed near −1.3 V (Figure 1b), which presumably corresponds to the reduction of the nitroaryl group.[17a] For complex **1f**, a second nonreversible process is also observed at 0.59 V, which possibly corresponds

(27) Conroy-Lewis, F. M.; Simpson, S. J. *J. Organomet. Chem.* **1987**, *322*, 221−228.

(28) Paul, F.; Toupet, L.; Roisnel, T.; Hamon, P.; Lapinte, C. *C. R. Chim.* **2005**, *8*, 1174−1185.

(29) Bruce, M. I.; Swincer, A. G.; Wallis, R. C. *J. Organomet. Chem.* **1979**, *171*, C5−C8.

(30) In accordance with such an assignment and as stated for **2a**, we overall observe a positive solvatochromic behavior for this transition in **1a** ($\Delta\lambda$ of ca. 50 nm between pentane and acetone).

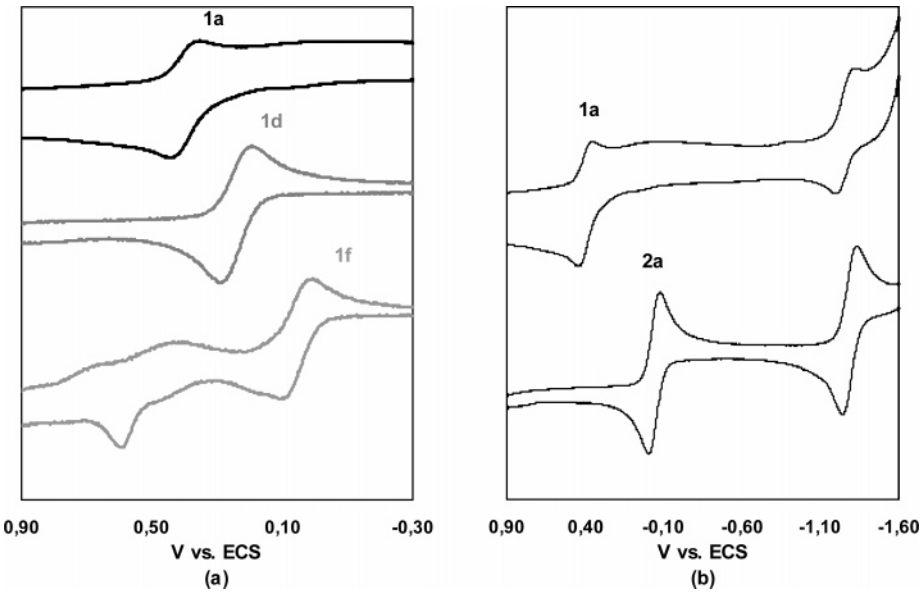

Figure 1. Cyclic voltammograms showing the metal-centered oxidations of (a) **1a** (X = NO_2), **1d** (X = H), and **1f** (X = NH_2) and (b) of **1a** and of the corresponding analogous Fe(II) complex **2a** in dichloromethane at 20 °C (0.1 M tetrabutylammonium hexafluorophosphate, scan rate 0.1 V/s).

Table 3. Electrochemical Data for (η^2-dppe)(η^5-C_5Me_5)Ru(C≡C-C_6H_4X) Complexes

X	ΔE_p (V)	E_0 (V)[a]	i_c/i_a[b]
4-NO_2 (**1a**)	0.09	0.40	>0.95
	0.12	−1.25	ca. 1.30
4-CN (**1b**)	0.08	0.36	>0.95
3-F (**1c**)	0.08	0.29	>0.80
4-F (**1c-*m***)	0.08	0.25	>0.85
4-H (**1d**)	0.09	0.23	>0.90
4-OMe (**1e**)	0.08	0.15	>0.95
4-NH_2 (**1f**)		0.59	nr[c]
	0.09	0.05	> 0.85

[a] All *E* values in V vs SCE. Conditions: CH_2Cl_2 solvent, 0.1 M [*n*-Bu_4N^+][PF_6^-] supporting electrolyte, 20 °C, Pt electrode, sweep rate 0.100 V s^{-1}. The ferrocene/ferrocenium couple (Fc/Fc^+) was used as an internal reference for potential measurements (Fc/Fc^+ taken at 0.460 V vs SCE in CH_2Cl_2).[33] [b] Ratio ±0.05. [c] Irreversible oxidation.

to the oxidation of the amino group (Figure 1a). Overall, very similar features were observed with the Fe(II) analogues **2a**−**f**, except that fully reversible electrochemical responses were obtained for the metal-centered oxidation for each substituent (Figure 1b).[17a]

X-ray Structures of Ru(II) Complexes. The para-substituted complexes **1a**−**f**, as well as the meta-substituted complex **1c-*m***, crystallize in triclinic or monoclinic space groups (Table 4, parts a−g of Figure 2), as previously observed with iron(II) analogues.[17c] The bond lengths and angles in the coordination sphere of the metal are the usual ones for such acetylide complexes (Table 5).[16,31] A noticeable change in comparison to previous structures is the conformation roughly perpendicular to the Ru/C_5 centroid adopted by the functional aryl ring in **1a**−**f** or **1c-*m***, while close-to-parallel conformations were previously observed with complexes possessing nonpermethylated cyclopentadienyl ligands.[31] On consideration of the comparatively high esds of **1c-*m***, no striking differences are apparent between the coordination spheres of the metal for the meta- and para-substituted fluoro complexes, the meta isomer having just a more bent acetylide bridge than the para isomer. More specifically along the series of para-substituted complexes, a lengthening of the Ru−C37 bond seems to take place on going from the most electron-withdrawing substituent (X = NO_2) to the most electron-releasing one (X = NH_2), from 1.997(6) Å for **1a** to 2.026(3) Å for **1f**. Although these changes are within the experimental error, their consistency suggests a real underlying effect. The acetylide bond apparently preserves its usual length around 1.22 Å but deviates somewhat from strict linearity (angle C37−C38−C39 ≠ 180°), as was also previously observed with iron(II) analogues. Concerning the various X substituents, the bond lengths are quite classical, given the reported esds.[32] The nitro, methoxy, and amino substituents in **1a**,**e**,**f** are roughly coplanar with the phenyl ring (dihedral angles for **1a**,**e**,**f**, respectively: C41−C42−N1−O1 = 12.2−10.1°; C41−C42−O1−C45 = −15.8°; C41−C42−N1−H = 1.8°), which suggests some slight π-interaction between these two fragments.

In Situ Study of Ru(III) Analogues. The observation of reversible or quasi-reversible peaks for the metal-centered oxidation led us to check if complexes **1a**$^+$−**1f**$^+$ were sufficiently stable to be isolated. We therefore tried first to isolate these species after chemical oxidation with silver(I) salts (Scheme 3).[33] Chemical oxidation was performed using a slight deficiency of silver triflate in dichloromethane followed by sonication to help dissolution of the triflate salt in dichloromethane. The oxidation reaction is signaled by a rapid color change of the reaction media. The intense color of the starting Ru(II) complexes bleaches upon addition of oxidant before turning darker, often blue in the case of strongly electron-releasing substituents. Unfortunately, all attempts at isolation of oxidized Ru(III) congeners failed. For instance, in the case of **1a**, dark red crystals could be recovered from the reaction

(31) (a) Powell, C. E.; Cifuentes, M. P.; McDonagh, A.; Hurst, S. K.; Lucas, N. T.; Delfs, C. A.; Stranger, R.; Humphrey, M. G.; Houbrechts, S.; Asselberghs, I.; Persoons, A.; Hockless, D. C. *Inorg. Chim. Acta* **2003**, *352*, 9−18. (b) Whittall, I. R.; Humphrey, M. G.; Hockless, D. C. R.; Skelton, B. W.; White, A. H. *Organometallics* **1995**, *14*, 3970−3979. (c) Bruce, M. I.; Humphrey, M. G.; Snow, M. R.; Tiekink, E. R. T. *J. Organomet. Chem.* **1986**, *314*, 213−225. (d) Wisner, J. M.; Bartczk, T. J.; Ibers, J. A. *Inorg. Chim. Acta* **1985**, *100*, 115−123.

(32) Allen, F. H.; Kennard, O.; Watson, D. G.; Brammer, L.; Orpen, A. G.; Taylor, R. *J. Chem. Soc., Perkin Trans. 2* **1987**, S1−S19.

(33) Connelly, N. G.; Geiger, W. E. *Chem. Rev.* **1996**, *96*, 877−910.

Table 4. Crystal Data, Data Collection, and Refinement Parameters for 1a−f and 1c-*m*

	1a (X = NO_2)	**1b** (X = CN)	**1c** (X = F)	**1c-*m*** (X = F)	**1d** (X = H)	**1e** (X = OMe)	**1f** (X = NH_2)
formula	$2(C_{44}H_{43}NO_2P_2Ru)\cdot CH_2Cl_2$	$C_{45}H_{43}NP_2Ru\cdot C_6H_6$	$C_{44}H_{43}FP_2Ru\cdot C_5H_{12}$	$C_{44}H_{43}FP_2Ru$	$C_{44}H_{44}P_2Ru\cdot H_2O$	$C_{45}H_{46}OP_2Ru$	$C_{44}H_{45}NP_2Ru$
fw	823.26	838.92	789.87	753.79	753.86	765.83	750.82
temp (K)	120(2)	293(2)	120(2)	293(2)	293(2)	150(2)	293(2)
cryst syst	triclinic	triclinic	triclinic	monoclinic	triclinic	monoclinic	monoclinic
space group	$P\bar{1}$	$P\bar{1}$	$P\bar{1}$	$P2_1/n$	$P\bar{1}$	$P2_1/c$	$P2_1/c$
a (Å)	12.8706(2)	12.3797(2)	11.9933(3)	8.7321(2)	12.026(5)	15.3442(2)	15.602(5)
b (Å)	14.6699(3)	13.5627(2)	12.0696(3)	19.3489(5)	12.072(5)	11.5119(1)	11.132(5)
c (Å)	22.5006(5)	14.3431(3)	15.8540(5)	22.1105(7)	15.671(5)	22.1852(3)	22.277(5)
α (deg)	89.720(1)	72.6573(8)	91.458(2)	90	73.609(5)	90	90
β (deg)	85.854(1)	88.1280(7)	104.174(1)	98.459(1)	89.080(5)	108.085(1)	108.800(5)
γ (deg)	66.620(1)	66.8617(8)	118.673(1)	90	61.644(5)	90	90
V (Å^3)	3888.1(1)	2104.03(6)	1924.5(1)	3695.1(1)	1901.9 (13)	3725.2(1)	3663(2)
Z	2	2	2	4	2	4	4
D_{calcd} (g cm^{-3})	1.406	1.324	1.363	1.355	1.320	1.365	1.362
cryst size (mm)	0.36 × 0.25 × 0.22	0.30 × 0.28 × 0.22	0.45 × 0.32 × 0.32	0.38 × 0.36 × 0.24	0.60 × 0.30 × 0.20	0.35 × 0.35 × 0.32	0.19 × 0.16 × 0.07
F(000)	1700	872	972	1560	784	1592	1560
diffractometer (NONIUS)	Kappa CCD	Kappa CCD	Kappa CCD	Kappa CCD	Kappa CCD	Kappa CCD	Kappa CCD
radiation	Mo Kα	Mo Kα	Mo Kα	Mo Kα	Mo Kα	Mo Kα	Mo Kα
abs coeff (mm^{-1})	0.593	0.484	0.528	0.546	0.528	0.541	0.548
data collection							
$2\theta_{max}$ (deg)	60	60	54	54	55	54	55
no. of frames	506	114	320	472	129	190	172
Ω rotation (deg)	0.8	2.0	2.0	0.6	2.0	1.6	1.6
frames/s	16	16	170	17	50	16	288
θ range (deg)	1.79−27.45	2.20−27.51	1.95−27.57	2.58−27.46	3.40−27.51	2.02−27.49	2.65−27.54
hkl ranges	0−16	0−16	−14 to +14	0−11	−15 to +15	0−19	−20 to +20
	−18 to +18	−15 to +17	−15 to +15	0−25	−15 to +15	0−14	−12 to +14
	−29 to +29	−18 to +18	−20 to +20	−28 to +28	−20 to +20	−28 to +28	−26 to +28
total no. of rflns	53 280	19 532	50 379	33 926	13 286	33 478	38 712
no. of unique rflns	17 060	9467	8864	8396	8516	8440	8338
no. of obsd rflns ($I > 2\sigma(I)$)	12 607	8183	7823	5446	6908	7348	5875
no. of restraints/params	0/926	0/497	0/467	0/443	0/443	0/443	0/434
$w = 1/[\sigma^2(F_o)^2 + (aP)^2 + bP]$[a]							
a	0.089	0.089	0.073	0.109	0.084	0.061	0.044
b	0	0	2.94	4.98	1.246	2.73	0.485
final *R*	0.073	0.035	0.044	0.068	0.0494	0.037	0.039
final R_w	0.183	0.087	0.118	0.164	0.1380	0.100	0.084
R (all data)	0.1041	0.044	0.0509	0.1214	0.0644	0.0454	0.0733
R_w (all data)	0.2032	0.094	0.1236	0.2005	0.1510	0.1075	0.0956
goodness of fit/F^2 (S_w)	1.069	1.063	0.999	1.023	1.059	1.070	1.035
$\Delta\rho_{max}$ (e Å^{-3})	3.02	0.65	0.67	1.2	1.1	1.1	0.4
largest diff peak, hole (e Å^{-3})	3.023, −2.268	0.646, −0.501	1.685, 1.262	1.247, 0.890	1.083, 0.728	1.018, −0.970	0.441, −0.400

[a] $P = [F_o^2 + F_c^2]/3$.

Scheme 3

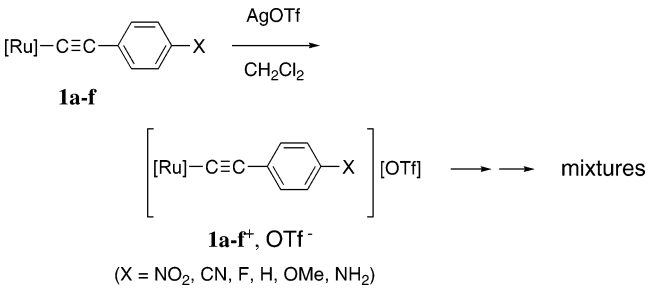

mixture, but these proved to correspond to the vinylidene triflate salt **6**[OTf][34] (Chart 2), rather than the desired **1a**[OTf].

Infrared monitoring suggests that the desired Ru(III) acetylide complex is the primary product, since a transient absorption around 1950 cm^{-1} develops (Table 1), which would typically correspond to the spectral signature expected for a Ru(III) ν(C≡C) band.[35] Unfortunately, the reaction mixture continues to change, yielding several new absorptions in the 1500−2000 cm^{-1} spectral range, while the Ru(III) ν(C≡C) band decreases. The presence of the carbonyl adduct **5**$^+$ (Chart 2) could never be evidenced at early stages,[25] possibly because no oxygen[28,35−36] or water[26,29,37] was available for its formation in the spectroscopic cell. Upon standing, the solution eventually returns to its original color and the re-formation of the starting Ru(II) complexes is observed with electron-withdrawing substituents.[38] After total decay of the Ru(III) ν(C≡C) band, NMR reveals the presence of several unidentified diamagnetic complexes in the medium, among which possibly lies the corresponding vinylidene salt.

ESR in dichloromethane/1,2-dichloroethane glasses at 80 K reveals that a single radical is generated following oxidation of the Ru(II) precursor using ferrocenium hexafluorophosphate. A rhombic signal (Figure 3), typical of a piano-stool metal-

(34) The identity of this complex was confirmed by a poor-quality X-ray diffraction study (see the Supporting Information).

(35) Adams, C. J.; Pope, S. J. A. *Inorg. Chem.* **2004**, *43*, 3492−3499.

(36) Choi, M.-Y.; Chan, M. C.-W.; Zhang, S.; Cheug, K.-K.; Che, C.-M.; Wong, K.-Y. *Organometallics* **1999**, *18*, 2074−2080.

(37) Le Lagadec, R.; Roman, E.; Toupet, L.; Müller, U.; Dixneuf, P. H. *Organometallics* **1994**, *13*, 5030−5039.

(38) This is notably the case for the nitro (**1a**) and cyano (**1b**) complexes (see the Supporting Information for an example).

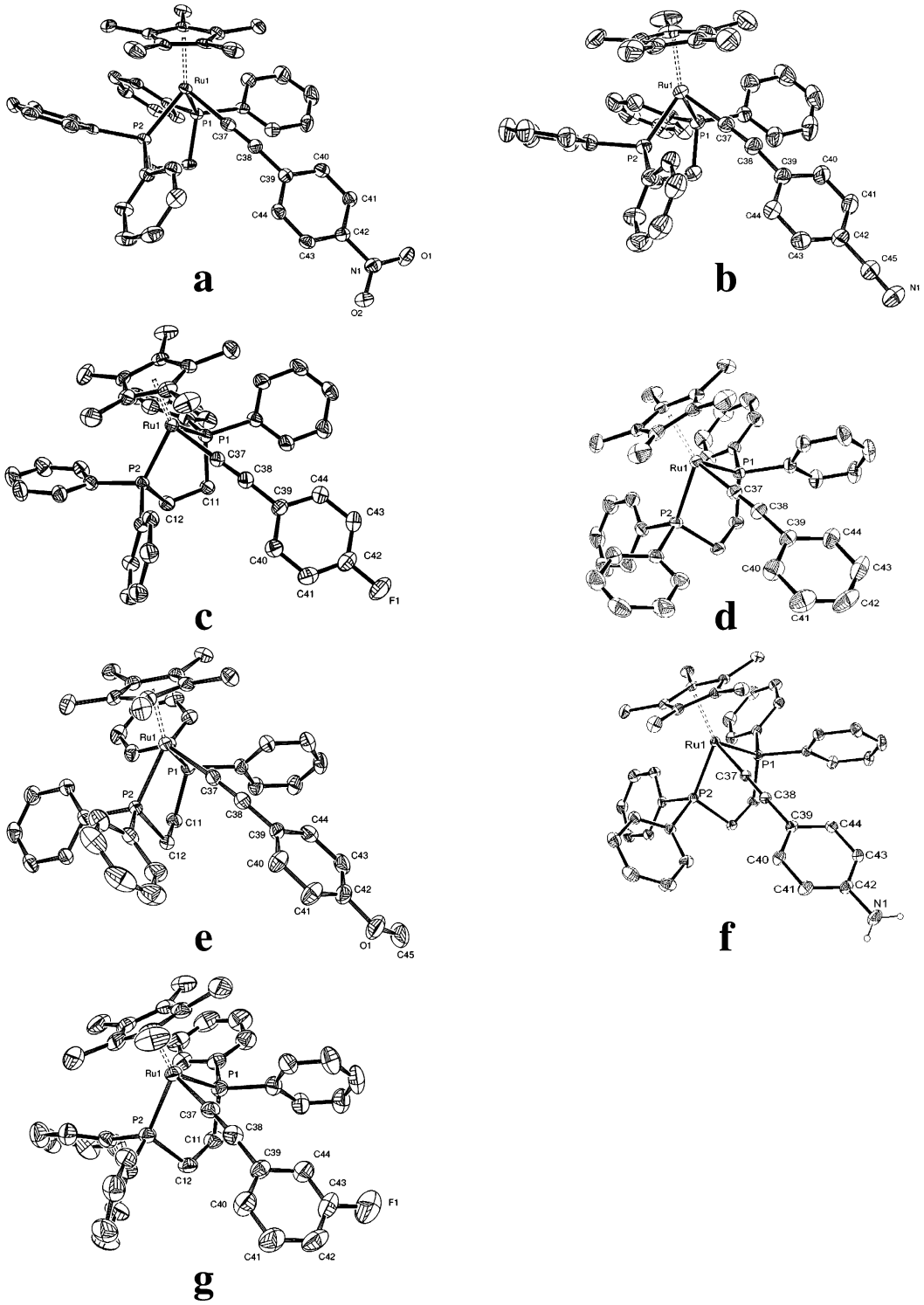

Figure 2. ORTEP plots (50% probability level) of (η^2-dppe)(η^5-C_5Me_5)Ru(C≡C)-1,4-(C_6H_4)X: (a) X = NO_2 (**1a**); (b) X = CN (**1b**); (c) X = F (**1c**); (d) X = H (**1d**); (e) X = OMe (**1e**); (f) X = NH_2 (**1f**); (g) (η^2-dppe)(η^5-C_5Me_5)Ru(C≡C)-1,3-(C_6H_4)F (**1c-*m***).

centered radical, is observed in each case (Table 6).[17d,39] No hyperfine structure is detected, but such features could easily be hidden underneath the signals observed for g_1, g_2, and g_3, which respectively have half-height widths of ca. 40, 50 and 70 G. With the most electron-releasing substituents, the ESR signal proved quite elusive when samples were warmed to room temperature, after thawing. The sample stability improves in the solvent glass. Thus, the signal of a sample of **1f**$^+$ (X = NH_2) in a vacuum-sealed ESR tube was monitored over 56 h at 77 K in a THF/dichloromethane (2:1) glass. The signal disappeared after 20 min at 300 K, dark residues being present in the tube after this period. At ambient temperature, an isotropic signal at $g = 2.04$ ($\Delta g = 26$ G peak to peak) could also be transiently observed with this sample. Possibly, the latter signal originates from an organic radical. The instability of these Ru(III) radicals is likely to be kinetic in origin. Moreover, the selective observation of one type of rhombic ESR signature for all compounds at low temperature suggests that oxidation essentially forms one metal-centered radical.

(39) Rieger, P. H. *Coord. Chem. Rev.* **1994**, *135/136*, 203−286.

Table 5. Selected Bond Lengths (Å) and Angles (deg) for 1a−f and 1c-*m*

	1a (X = NO_2)[a]	**1b** (X = CN)	**1c** (X = F)	**1c-*m*** (X = F)	**1d** (X = H)	**1e** (X = OMe)	**1f** (X = NH_2)
			Selected Bond Lengths				
Ru−$(Cp^*)_{centroid}$	1.891/1.889	1.895	1.890	1.895	1.884	1.894	1.901
Ru−P1	2.2639(14)/2.2676(14)	2.2639(5)	2.2583(7)	2.2663(14)	2.2622(12)	2.2652(2)	2.2622(11)
Ru−P2	2.2747(14)/2.2650(15)	2.2755(6)	2.2715(7)	2.2709(13)	2.2563(12)	2.2643(6)	2.2625(11)
Ru−C37	1.997(6)/2.004(6)	2.004(2)	2.014(3)	2.017(5)	2.011(4)	2.015(2)	2.026(3)
C37−C38	1.221(8)/1.225(8)	1.209(3)	1.209(4)	1.195(7)	1.215(5)	1.216(3)	1.202(4)
C38−C39	1.437(8)/1.413(8)	1.434(3)	1.445(4)	1.441(7)	1.431(5)	1.433(3)	1.444(4)
C39−C40	1.410(8)/1.405(8)	1.399(3)	1.404(4)	1.383(9)	1.394(6)	1.398(4)	1.399(4)
C40−C41	1.379(8)/1.379(8)	1.379(4)	1.392(4)	1.393(9)	1.380(7)	1.382(4)	1.383(4)
C41−C42	1.389(8)/1.382(8)	1.390(4)	1.373(5)	1.374(11)	1.358(9)	1.366(4)	1.379(5)
C42−C43	1.384(8)/1.383(8)	1.387(3)	1.362(5)	1.369(11)	1.332(9)	1.382(4)	1.389(5)
C43−C44	1.379(8)/1.380(8)	1.379(3)	1,386(5)	1.342(8)	1.379(7)	1.398(4)	1.384(4)
C44−C39	1.403(8)/1.411(8)	1.401(3)	1.404(4)	1.408(8)	1.387(6)	1.399(4)	1.388(4)
C42−F1			1.365(4)	1.337(8)			
C42−O1						1.379(3)	
C45−O1						1.410(4)	
C42−C45		1.435(4)					
N1−C45		1.137(4)					
C42−N1	1.465(7)/1.456(8)						1.404(4)
N1−O1	1.232(7)/1.232(7)						
N1−O2	1.227(7)/1.235(7)						
			Selected Bond Angles				
P1−Ru−P2	83.58(5)/83.63(5)	83.78(2)	83.65(3)	84.02(5)	83.73(4)	83.01(2)	83.12(3)
P1−Ru−C37	82.33(16)/86.94(16)	80.50(6)	80.24(8)	82.78(15)	85.37(11)	85.57(7)	79.10(8)
P2−Ru−C37	87.16(16)/82.56(16)	85.09(6)	85.76(8)	80.92 (14)	81.67(11)	79.01(6)	85.46(8)
Ru−C37−C38	178.8(5)/177.9(5)	176.9(2)	178.9(3)	172.9(4)	179.1(3)	175.4(2)	176.1(3)
C37−C38−C39	171.6(6)/172.2(6)	172.1(3)	172.6(3)	172.9(5)	173.7(4)	171.1(3)	172.7(3)
C40−C39−C44	120.7(5)/117.9(5)	117.5(2)	117.7(3)	117.3(5)	116.6(4)	116.9(2)	116.6(3)
C41−C42−C43	122.2(5)/122.2(5)	119.2(2)	123.1(3)	117.5(6)	119.6(5)	119.9(2)	118.3(3)
C41−C42−F1			118.2(3)	118.2(6)			
C43−C42−F1			118.7(3)	117.3(7)			
C41−C42−O1						115.7(3)	
C43−C42−O1						124.5(3)	
C42−O1−C45						116.9(3)	
C41−C42−N1	118.5(5)/119.4(5)						121.2(3)
C43−C42−N1	119.3(5)/118.4(5)						120.5(3)
C42−C45−N1		177.7(4)					
O1−N1−O2	123.2(5)/122.9(6)						
Ru−$(Cp^*)_{centroid}$/C39−C40[b]	−71.47/−73.19	−91.8	110.2	−108.7	−108.5	−104.8	−104.2

[a] Two molecules in the asymmetric unit. [b] Dihedral angle in degrees (Cp* = pentamethylcyclopentadienyl ligand).

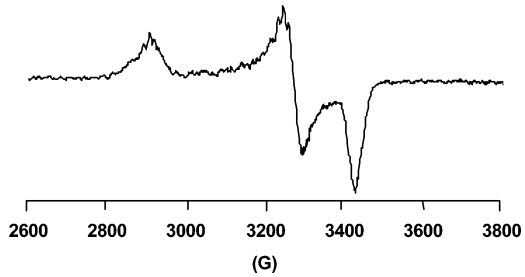

Figure 3. ESR spectrum of the **1b**[PF_6] radical (X = CN) in 1,2-CH_2Cl_2/$C_2H_4Cl_2$ (1:1) at 80 K.

Table 6. ESR Spectroscopic Data[a] for [(η^2-dppe)(η^5-C_5Me_5)Ru(C≡C-C_6H_4X)][PF_6] Complexes

X	g_1	g_2	g_3	$\langle g \rangle$	Δg
4-NO_2 (**1a**$^+$)	1.971	2.067	2.333	2.123	0.362
4-NO_2 (**1a**$^+$)[b]	1.973	2.069	2.320	2.120	0.347
4-CN (**1b**$^+$)	1.973	2.068	2.327	2.123	0.354
3-F (**1c-*m***$^+$)[c]	1.980	2.064	2.301	2.115	0.321
4-F (**1c**$^+$)	1.985	2.063	2.279	2.109	0.294
4-H (**1d**$^+$)	1.988	2.057	2.227	2.091	0.239
4-OMe (**1e**$^+$)	1.990	2.059	2.239	2.096	0.249
4-NH_2 (**1f**$^+$)	1.998	2.043	2.145	2.062	0.135
4-NH_2 (**1f**$^+$)[b]	1.998	2.040	2.131	2.056	0.142

[a] At 77 or 80 K in CH_2Cl_2−$C_2H_4Cl_2$ (1:1) glass. [b] At 77 or 80 K in CH_2Cl_2−THF (1:2) glass. [c] 1,3-substituted isomer.

These Ru(III) radical cations could also be characterized by electronic spectroscopy at ambient temperature (300 K) in dichloromethane. On the basis of previous work with Fe(III) analogues,[17d] we anticipated that these radical species should present a weak but characteristic absorption in the near-IR range, corresponding to a forbidden LF transition. After chemical oxidation, assessed by its diagnostic color change, a weak absorption around 1300 nm was observed each time (Table 7, Figure 4), except in the case of the amino complex **1f**$^+$. Expectedly, this weak spectral feature disappears upon standing. It was also confirmed that neither the starting Ru(II) parent complex nor the silver triflate has absorptions in this spectral range. For the amino complex **1f**$^+$, the missing absorption is either hidden (it could correspond to a very weak shoulder around 1050 ± 50 nm on the low-energy side of the absorption detected at 813 nm) or not detected at all. The extinction coefficients reported for these bands in Table 5 were computed by considering a total conversion of the initial Ru(III) complexes. As a consequence, these "apparent" values are lower than the real ones, since the actual concentration of the Ru(III) radicals present in the cell is evidently lower.

Transient absorptions could also be observed in the UV−visible range. Given the number of species which are generated by oxidation and which are likely to absorb in this spectral region, no definitive data concerning the Ru(III) radical data could be obtained from these experiments. There are, however, strong analogies between the transient absorptions immediately observed following oxidation (Supporting Information) and those previously reported for the stable Fe(III) analogues.[17d]

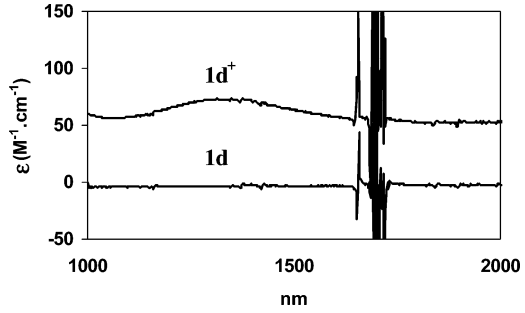

Figure 4. Near-IR spectra of **1d** and **1d**[OTf] in CH_2Cl_2.

Table 7. Solution[a] Near-IR Data for [(η^2-dppe)(η^5-C_5Me_5)Ru(C≡C)-1,4-(C_6H_4)X][OTf]

X	$\nu_{max} \pm 25^b$ ($\epsilon \pm 5^c$)
NO_2 (**1a**$^+$)	1430/6990 (144)
CN (**1b**$^+$)	1370/7300 (90)
F (**1c**$^+$)	1310/7630 (300)
H (**1d**$^+$)	1330/7520 (23)
OMe (**1e**$^+$)	1240/8070 (82)
NH_2 (**1f**$^+$)	nd[d]

[a] In CH_2Cl_2 in the absorbance mode at 20 °C. [b] Given in nm/cm^{-1}. [c] Tentative estimate in M^{-1} cm^{-1} (see text). [d] Not detected.

Table 8. Selected Bond Distances Computed for (PH_3)$_2$(η^5-C_5H_5)Ru(C≡C)-1,4-(C_6H_4)X (1a-H/1d-H/1f-H) Compared to the X-ray Data Available for the Complexes (η^2-dppe)(η^5-C_5Me_5)Ru(C≡C)-1,4-(C_6H_4)X/ (η^2-dppe)(η^5-C_5H_5)Ru(C≡C)-1,4-(C_6H_4)X/ (Ph_3P)$_2$(η^5-C_5H_5)Ru(C≡C)-1,4-(C_6H_4)X (X = NO_2, H, NH_2)[a]

	1a-H (X = NO_2)	**1d**-H (X = H)	**1f**-H (X = NH_2)
Ru−C37	2.02 (2.00[b]/1.99[c]/1.99[d])	2.03 (2.01/2.01[e]/2.02[e])	2.04 (2.03)
C37−C38	1.23 (1.22[b]/1.21[c]/1.20[d])	1.23 (1.21/1.20[e]/1.21[e])	1.23 (1.20)
C38−C39	1.42 (1.44[b]/1.42[c]/1.43[d])	1.43 (1.43/1.44[e]/1.46[e])	1.43 (1.44)
C39−C40	1.42 (1.41[b]//1.43[d])	1.42 (1.39)	1.42 (1.40)
C40−C41	1.39 (1.38[b]//1.41[d])	1.39 (1.38)	1.39 (1.38)
C41−C42	1.40 (1.39[b]//1.37[d])	1.40 (1.35)	1.40 (1.39)
C42−C43	1.40 (1.38[b]//1.36[d])	1.40 (1.33)	1.40 (1.39)
C43−C44	1.39 (1.38[b]//1.37[d])	1.39 (1.38)	1.39 (1.38)
C44−C45	1.42 (1.40[b]//1.40[d])	1.42 (1.39)	1.42 (1.39)
Ru−(Cp)[f]	1.96 (1.89[b])	1.99 (1.88)	1.98 (1.90)
Ru−P1	2.31 (2.26[b]//2.30[d])	2.29 (2.26/2.24[e]/2.31[e])	2.30 (2.26)
Ru−P2	2.31 (2.27[b]//2.30[d])	2.29 (2.25/2.25[e]/2.29[e])	2.30 (2.26)
C42−X	1.46 (1.47[b]//1.47[d])	/	1.41 (1.40)
δ[g]	88 (71[b])	88 (108)	88 (104)

[a] Refer to Figure 2 for labeling (experimental values are given in parentheses). [b] Experimental value given for a selected molecule in the asymmetric unit of **1a**. [c] Values taken from ref 31b. [d] Values taken from ref 31a. [e] Values taken from ref 31c. [f] (Cp) = Cp centroid. [g] Dihedral angle Fe−(Cp)−C1−C6.

DFT Computations on Model Compounds. Theoretical computations on the model Ru(II/III) complexes **1a**-H/**1a**-H$^+$ (X = NO_2), **1f**-H/**1f**-H$^+$ (X = H), and **1j**-H/**1j**-H$^+$ (X = NH_2), where the chelating dppe ligand has been replaced by two PH_3 ligands and where the C_5Me_5 ligand has been replaced by C_5H_5, have been performed.[40] The optimized bond lengths and angles, obtained without symmetry constraints, match quite well not only the geometric features of the (η^2-dppe)(η^5-C_5Me_5)Ru-(C≡C)-1,4-(C_6H_4)X complexes presently obtained in the solid state but also those previously published for some (η^2-dppe)-(η^5-C_5H_5)Ru(C≡C)-1,4-(C_6H_4)X and (Ph_3P)$_2$(η^5-C_5H_5)Ru-(C≡C)-1,4-(C_6H_4)X complexes (X = NO_2, H; Table 8).[31] Notably, the slight increase in the Ru−C bond length theoretically computed, on proceeding from a nitro (**1a**-H) to an amino (**1f**-H) substituent, is apparently reproduced in the available solid-state data,[31] although these changes remain below the experimental uncertainty with **1a**−**f**. Geometric optimizations confirm that the most stable configuration is that where the functional aryl ring is roughly parallel to the Cp plane (see X-ray structures) but also suggest that rotation of the functional aryl group around the acetylide axis should be easy in solution. Energies of the frontier MOs for Ru(II) complexes are shown in Figure 5, and their orbital composition is given in Table 9. The NO_2-containing complex shows a smaller HOMO−LUMO gap due to an empty MO (52a) essentially localized on the NO_2 fragment which lies between the HOMO (50a) and the first antibonding MO centered on the metal (53a). Without this particular MO, the HOMO−LUMO gap would slightly decrease on going from the most electron-withdrawing substituent to the most electron-releasing one.

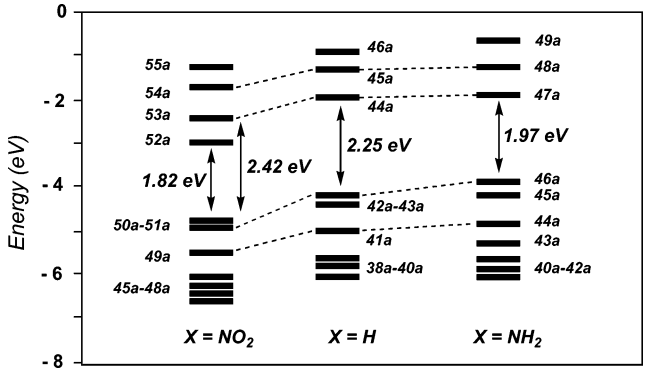

Figure 5. Energy (eV) of the frontier MOs of the (H_3P)$_2$(η^5-C_5H_5)-Ru(C≡C)-1,4-(C_6H_4)X model complexes **1a**-H (X = NO_2), **1d**-H (X = H), and **1f**-H (X = NH_2).

Two closely lying MOs with sizable metal acetylide character (ca. 16−43% and 33−43%, respectively) constitute the HOMO and HOMO − 1 of these Ru(II) complexes. These MOs roughly correspond to the perpendicular π-manifolds on the acetylide ligand. The HOMO corresponds to the π-manifold conjugated with the X substituent for the compounds **1d**-H and **1f**-H, containing the most electron releasing groups (X = H, NH_2), as observed for the Fe(II) analogues.[17c] This MO is stabilized with the nitro substituent and constitutes the HOMO − 1 in complex **1a**-H (X = NO_2; Figure 5). This illustrates the influence of the X substituent on the π-bonding in these compounds. Additionally, the phenylacetylide character of these two MOs slightly increases, with a concomitant decrease in Ru character, on going from the nitro (**1a**-H) to the amino (**1f**-H) complexes (see Table 9). For all of the systems except for X = NO_2, the LUMO is an Ru−Cp antibonding orbital, while for X = NO_2 (**1a**-H), the corresponding MO is the LUMO + 1, 0.50 eV higher in energy than the LUMO, which is localized on the aryl-NO_2 moiety.

The Ru−C bond dissociation energies were next computed for the Ru(II) complexes bearing the most electron-withdrawing substituents (**1a**-H, X = NO_2; **1b**-H, X = CN). These were obtained from complexes with idealized C_s symmetry, considering a heterolytic process, i.e. the bond dissociation energy (BDE) between [(H_3P)$_2$(η^5-C_5H_5)Ru]$^+$ and [(C≡C)-1,4-(C_6H_4)X]$^-$ fragments, according to the general *transition state* method of Ziegler and Rauk,[42,43] as previously done for the Fe(II) analogues.[17c] The data are given in Table 10 along with the results previously obtained for the Fe(II) analogues. The two families of complexes have very similar bond dissociation energies, and all energetic terms compare quite well. Apparently,

(40) DFT computations on similar model compounds have been performed by Koentjoro et al. and Powell et al. in the framework of larger theoretical investigations, but the detailed MO compositions (in terms of AOs) of these compounds were not published.[31a,41]

Table 9. Energy, Electron Occupancy, and Decomposition of Frontier MOs in $(PH_3)_2(\eta^5\text{-}C_5H_5)Ru(C{\equiv}C)\text{-}1,4\text{-}(C_6H_4)X$ Model Complexes (X = NO_2, H, NH_2)[a]

Compound **1a**-H (X = NO_2)

	MO								
	55a	54a	53a	52a	51a	50a	49a	48a	47a
ϵ (eV)	−1.27	−1.72	−2.39	−2.98	−4.81	−4.89	−5.52	−6.15	−6.28
occ	0	0	0	0	2	2	2	2	2
% Ru	0	46	44	1	43S	32	48	0	53
% C (Cp)	0	18	26	0	7	0	19	0	0
% P	0	16	29	0	1	1	4	0	0
% C_α	0	15	0	6	10	12	6	0	9
% C_β	0	4	0	0	27	21	2	0	0
% C (Ph)	99	0	0	27	0	17	1	0	16
% NO_2	0	0	0	63	0	4	0	96	0

Compound **1d**-H (X = H)

	MO								
	47a	46a	45a	44a	43a	42a	41a	40a	39a
ϵ (eV)	−0.73	−0.98	−1.36	−2.03	−4.28	−4.35	−5.07	−5.75	−5.78
occ	0	0	0	0	2	2	2	2	2
% Ru	23	2	47	46	27	40	47	57	0
% C (Cp)	3	0	8	25	0	6	17	0	0
% P	48	0	14	30	0	0	4	0	0
% C_α	5	15	17	0	17	12	6	5	0
% C_β	0	2	4	0	21	28	1	0	0
% C (Ph)	0	80	0	0	24	0	4	20	97

Compound **1f**-H (X = NH_2)

	MO								
	50a	49a	48a	47a	46a	45a	44a	43a	42a
ϵ (eV)	−0.63	−0.67	−1.24	−1.20	−3.89	−4.21	−4.89	−5.31	−5.72
occ	0	0	0	0	2	2	2	2	2
% Ru	0	20	43	51	16	39	49	40	0
% C (Cp)	0	3	7	25	0	6	14	3	0
% P	0	23	29	29	0	0	1	1	0
% C_α	0	3	15	0	18	13	3	1	0
% C_β	0	0	4	0	15	28	0	8	0
% C (Ph)	98	16	0	0	30	0	9	17	94
% NH_2	0	0	0	0	8	0	4	12	0

[a] "0" means less than 1%.

Table 10. Heterolytic Bond Dissociation Energies and Energy Decomposition of the M−C Bond in $(PH_3)_2(\eta^5\text{-}C_5H_5)M(C{\equiv}C)\text{-}1,4\text{-}(C_6H_4)X$ Complexes (M = Ru, Fe; X = NO_2, CN)

	M = Ru		M = Fe	
	X = NO_2	X = CN	X = NO_2	X = CN
ΔE_{Pauli}	−8.86	−8.60	−7.37	−7.37
ΔE_{orb}[a]	+4.44	+4.39	+3.82	+3.97
ΔE_σ	+2.38	+2.77	+1.74	+1.95
$\Delta E_{\pi,M\to L}$	+1.68	+1.60	+1.68	+1.59
$\Delta E_{\pi,L\to M}$	+0.41	+0.42	+0.40	+0.43
ΔE_{el}	+10.77	+10.88	+10.20	+10.19
BDE (ΔH)	+6.55	+6.76	+6.66	+6.77

[a] $\Delta E_{orb} = \Delta E_\sigma + \Delta E_{\pi,M\to L} + \Delta E_{\pi,L\to M}$.

the Ru(II) complexes present a somewhat larger orbital σ-stabilizing contribution (ΔE_{orb}), which is compensated by a larger destabilizing Pauli term (ΔE_{Pauli}).

Upon oxidation, the electron is removed from a delocalized molecular orbital, being more and more heavily weighted on the metal center (i.e. 16/27/43% for **1f**-H/**1d**-H/**1a**-H) as the substituent is becoming more and more electron-withdrawing. The effect of oxidation on the energies of the molecular orbitals is depicted in Figure 6 for **1d** and **1d**-H^+ (X = H). As can be seen in this diagram, the HOMO−LUMO gap slightly increases upon oxidation. In the Ru(III) model complexes, the LUMO for these electron-rich compounds has a dominant d_{xy} character and the LUMO + 1 a dominant d_{z^2} character. The SOMO, and the two MOs below correspond to the "t_{2g}" set of the Fe(III) ion (pseudo-O_h symmetry). The SOMO and SOMO − 1, however, retain their important acetylide character (Table 11).

The energies of the six frontier spin MOs (α and β) possessing a sizable metal character in **1a**-H^+−**1f**-H^+ (two unoccupied and four occupied) are shown in Figure 7. The metal contribution to the higher lying spin MOs is dominated by one type of d atomic orbital (Table 11). In contrast, the metal contribution to the lower lying ones is more accurately described by a mixture of two d AOs. In the case of the complex **1a**-H^+, three aryl- and nitro-based MOs are found between the filled-spin MOs.

The spin distributions computed for **1a**-H^+, **1d**-H^+, and **1f**-H^+ are given in Table 12. The largest positive spin density is found on the metal and, to a lesser extent, on the β-carbon atom of the acetylide. It is strongly influenced by the X substituent, being larger on these two atoms with the most electron-withdrawing substituents. The spin delocalization on the aryl-acetylide fragment is clearly favored for the most electron-releasing substituents, spreading more and more on the aryl

(41) Koentjoro, O. F.; Rousseau, R.; Low, P. J. *Organometallics* **2001**, *20*, 4502−4509.
(42) Ziegler, T.; Rauk, A. *Inorg. Chem.* **1979**, *18*, 1558−1565.
(43) Bickelhaupt, F. M.; Baerends, E. J. In *Reviews of Computational Chemistry*; Lipkowitz, K. B., Boyd, D. B., Eds.; Wiley: New York, 2000; Vol. 15, pp 1−86.

Table 11. Decomposition of Frontier MOs in $[(PH_3)_2(\eta^5\text{-}C_5H_5)Ru(C{\equiv}C)\text{-}1,4\text{-}(C_6H_4)X]^+$ Model Complexes (X = NO_2, H, NH_2) for Selected Frontier MOs[a]

Compound **1a**-H^+ (X = NO_2)

	MO											
	54a(α)	54a(β)	52a(α)	52a(β)	51a(α)	51a(β)	50a(α)	50a(β)	48a(α)	49a(β)	45a(α)	45a(β)
ϵ (eV)	−5.55	−5.46	−6.21	−6.11	−8.77	−8.47	−8.98	−8.62	−9.33	−9.20	−10.18	−10.00
occ	0	0	0	0	1	0	1	1	1	1	1	1
% Ru	43	45	47	33	36	33	27	39	52	46	47	47
% Cp	11	20	28	21	4	2	5	5	25	19	8	4
% P	9	10	24	19	0	0	0	1	3	2	0	0
% C_α	15	15	0	2	10	12	9	10	4	5	4	7
% C_β	3	3	0	0	23	21	19	23	1	0	0	0
% C (Ar)	0	0	0	7	13	16	17	9	0	0	23	25
% NO_2	0	0	0	13	0	0	1	0	0	12	0	0

Compound **1d**-H^+ (X = H)

	MO											
	45a(α)	45a(β)	44a(α)	44a(β)	43a(α)	43a(β)	42a(α)	42a(β)	41a(α)	41a(β)	39a(α)	39a(β)
ϵ (eV)	−5.20	−5.11	−5.80	−5.72	−8.33	−8.00	−8.50	−8.21	−8.88	−8.76	−9.77	−9.53
occ	0	0	0	0	1	0	1	1	1	1	1	1
% Ru	40	44	49	44	43	28	27	43	52	52	23	49
% Cp	19	20	27	27	7	0	0	7	24	23	9	3
% P	6	8	24	24	3	0	0	2	3	3	0	0
% C_α	16	16	0	0	8	14	13	9	5	6	4	6
% C_β	3	4	0	0	25	19	16	1	1	1	0	0
% C (Ph)	3	0	0	0	1	24	29	0	0	0	23	27

Compound **1f**-H^+ (X = NH_2)

	MO											
	48a(α)	48a(β)	47a(α)	47a(β)	46a(α)	46a(β)	45a(α)	45a(β)	44a(α)	44a(β)	43a(α)	43a(β)
ϵ (eV)	−4.70	−5.60	−5.25	−5.19	−7.74	−7.34	−7.82	−7.74	−8.34	−8.23	−8.99	−8.75
occ	0	0	0	0	1	0	1	1	1	1	1	1
% Ru	41	44	43	44	21	20	45	45	52	50	45	45
% Cp	15	20	28	27	0	0	9	8	25	23	0	0
% P	4	11	25	23	0	0	2	1	5	2	0	0
% C_α	17	15	0	0	14	15	7	7	5	4	0	0
% C_β	4	4	0	0	12	14	25	25	1	1	5	6
% C (Ar)	18	0	0	0	33	32	0	0	0	2	21	21
% NH_2	2	0	0	0	12	11	0	0	1	2	13	13

[a] "0" means less than 1%.

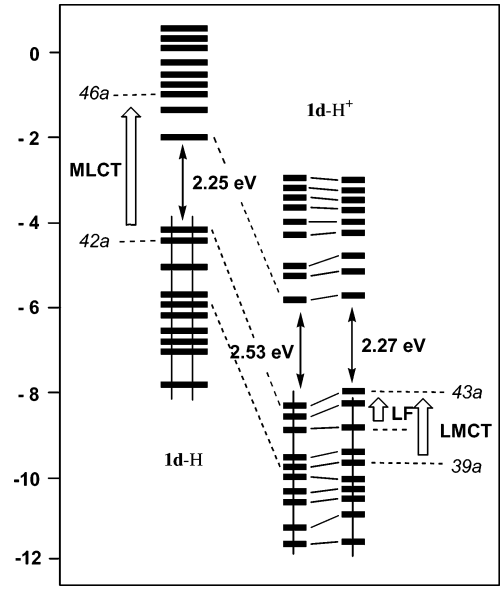

Figure 6. Orbital diagram for $[(H_3P)_2(\eta^5\text{-}C_5H_5)Ru(C{\equiv}CC_6H_5)]^{0/+}$ (**1d**-H/**1d**-H^+) showing the effect of oxidation on the energy levels (eV). The arrows indicate the possible excitations leading to MLCT, LMCT, or LF transitions in the visible range.

ring.[44] This shows that the spatial localization of the unpaired spin density in the arylacetylide is strongly tuned by the substituent.

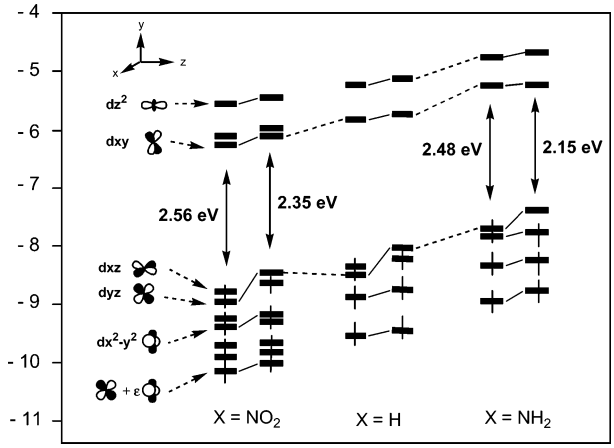

Figure 7. Energy (eV) of the frontier molecular spin orbitals of the model complexes $[(H_3P)_2(\eta^5\text{-}C_5H_5)Ru(C{\equiv}C)\text{-}1,4\text{-}(C_6H_4)X]^+$ (**1a**-H^+−**1c**-H^+; X = NO_2, H, NH_2). Metallic AOs involved in frontier MOs having a sizable metallic character are shown on the left-hand side. In the case of **1a**-H^+ (X = NO_2), intercalating nitro-based MOs are also shown.

Overall, these theoretical results support and usefully complement recent DFT calculations of Rousseau and Low[41] and of Humphrey and Stranger[31a] on similar model compounds.[40]

Correlations of Characteristic CV and Spectroscopic Data with ESPs. A very good correlation (R^2 = 0.99) is obtained

Table 12. Calculated Spin Densities for $[(PH_3)_2(\eta^5\text{-}C_5H_5)Ru(C{\equiv}C)\text{-}1,4\text{-}(C_6H_4)X]^+$ Complexes (X = NO_2, CN, Br, H, OMe, NH_2)

	1a-H^+ (X = NO_2)	**1d**-H^+ (X = H)	**1f**-H^+ (X = NH_2)
Ru	0.405	0.352	0.242
C_α	0.077	0.138	0.187
C_β	0.295	0.243	0.143
$-1,4\text{-}C_6H_4-$	0.165	0.277	0.323
X	0.018	−0.012	0.126
C_5H_5	0.015	0.005	−0.004
2 PH_3	0.026	−0.001	−0.005

between the σ Hammett ESPs[45,46] and the redox potentials corresponding to the Ru(II)/Ru(III) oxidation of **1a**−**f** (eq 1 and

$$E_0\,(\mathrm{V}) = 0.235\sigma + 0.217 \quad (1)$$

Figure 8a). Notably, the inclusion of the data for the meta-substituted complex **1c**-*m* does not change the quality of the linear fit. The positive slope reflects the fact that an electron-releasing substituent renders the ruthenium-centered oxidation more facile. The linear correlation evidences an essentially electronic substituent effect.

In addition, significant linear fits are also obtained with the acetylide stretch expressed in cm^{-1} ($R^2 = 0.96$), the energy (in cm^{-1}) of the lowest-lying electronic (MLCT) transition ($R^2 = 0.95$), and the ^{13}C NMR shifts of the α- ($R^2 = 0.96$) or β-carbons ($R^2 = 0.93$) of the acetylide ligand vs the σ^- ESPs (eqs 2−4).

$$\nu_{C\equiv C}\,(\mathrm{cm}^{-1}) = -25.8\sigma^- + 2070 \quad (2)$$

$$E_{MLCT}\,(\mathrm{cm}^{-1}) = -7944\sigma^- + 31\,862 \quad (3)$$

$$\delta(C_\alpha)\,(\mathrm{ppm}) = 19.1\sigma^- + 127 \quad (4a)$$

$$\delta(C_\beta)\,(\mathrm{ppm}) = 3.1\sigma^- + 110 \quad (4b)$$

Poorer linear fits were obtained in these correlations when the regular Hammett ESPs (σ) were used, as previously found for Fe(II) acetylides.[17c] The use of σ^- reveals the dominance of mesomeric interactions in these substituent effects.

In the case of Ru(III) complexes some linear correlations could also be obtained with ESR data (parts a and b of Figure 9). This has already been noted for Fe(III) analogues.[17d] More remarkably, better fits were obtained in these cases with Hammett ESPs rather than with σ^+ ESPs, suggesting a more balanced influence of the substituent mesomeric and inductive effects. The equations of the linear fits for $\langle g\rangle$ and Δg are given in eqs 5a,b.

$$\langle g\rangle = 0.0402\sigma_p + 2.0975 \quad (5a)$$

$$\Delta g = 0.1496\sigma_p + 0.2597 \quad (5b)$$

Derivation of Hammett Electronic Substituent Parameters (ESP's) of the "$(\eta^2$-dppe$)(\eta^5\text{-}C_5Me_5)$Ru−C≡C−" Fragment. As previously done for the "$(\eta^2$-dppe$)(\eta^5\text{-}C_5Me_5)$Fe(C≡C)−" fragment,[24] we have derived experimentally the Hammett ESP's of the "$(\eta^2$-dppe$)(\eta^5\text{-}C_5Me_5)$Ru−C≡C−" fragment by means of ^{19}F NMR, using the simple procedure described by Taft and co-workers (Experimental Section).[47] The measurement gives values of −0.40 and −0.47 for σ_m and σ_p,[45,46] respectively, which indicates a quite strong electron-releasing character for the "$(\eta^2$-dppe$)(\eta^5\text{-}C_5Me_5)$Ru−C≡C−" fragment. This organo-ruthenium(II) substituent apparently behaves as an electron-releasing group via both the π- and σ-molecular orbital manifolds, as suggested by the values of the inductive ($\sigma_I = -0.33$) and resonance ($\sigma_R = -0.09$) contributions. Such electron-releasing capabilities are in fact slightly higher than those derived for the analogous Fe(II) fragment ($\sigma_m = -0.29$ and $\sigma_p = -0.37$). Notably, these values are significantly lower than the σ_p value of −0.81 previously derived by Sato and co-workers for the "$(Ph_3P)_2(\eta^5\text{-}C_5H_5)$Ru−C≡C−" fragment by electrochemical means.[48]

Discussion

In the following, we will compare the data obtained for **1a**−**f**/**1a**−**f**$^+$ and **1a**−**f**-H/**1a**−**f**-H^+ with these previously obtained for the corresponding Fe(II) analogues (**2a**−**f**/**2a**−**f**$^+$ and **2a**−**f**-H/**2a**−**f**-H^+)[17] in order to determine the influence of the nature of the metal on the bonding and reactivity of these compounds, in line with related investigations.

Ru(II) Complexes. The bonding in this series of Ru(II) complexes strongly resembles that previously found for the series of Fe(II) analogues (Figure 10)[17c] with, however, slightly increased acetylide character in the HOMO and HOMO − 1. Thus, replacing the Fe(II) center by the more electronegative Ru(II) center does not drastically change the bonding in these electron-rich d^6 piano-stool acetylide complexes but results in more delocalized frontier MOs. Since we anticipated that changing the metal center should affect back-bonding, we tried to derive its magnitude for Ru(II) complexes bearing electron-withdrawing groups such as **1a**-H and **1b**-H (X = NO_2, CN), as previously done for **2a**−**f**-H.[17c] Although the latter is weak in a bonding scheme dominated by filled−filled (repulsive) interactions between the d MOs on the Ru(II) fragment and π MOs of the acetylide fragment,[15b,31a] back-bonding should become sizable with electron-withdrawing substituents.[18,49] The energetic importance of back-bonding on the Ru−C bond is given by the $\Delta E_{\pi,M\to L}$ term in Table 10 (i.e. bonding contributions to the BDE),[49,50] The latter does not change much between **1a**-H and **1b**-H (X = NO_2, CN) and, in contrast to our initial expectations, compares quite well with values previously derived for the Fe(II) analogues. Such a statement is in line with the computations of Stranger and co-workers, who found close values for back-donation in related Fe(II) and Ru(II) acetylide analogues.[18] It evidences that back-bonding cannot be envisioned as the primary cause of the large hyperpolarizabilities measured by EFISH for these compounds.[12] Dissociation energies derived for the M−C bonds in these compounds are also quite close.

(44) As a result of the avoided crossing mentioned above, the unpaired spin density is located in the π-manifold conjugated with the aryl ring for the compounds bearing the electron-releasing substituents and in the perpendicular π-manifold for the electron-accepting X substituents, while for compounds with moderate substituents such as **1f**-H^+, the spin density is located around the acetylide bridge in both π_x- and π_y-manifolds. See ref 17d for an analogous behavior.

(45) March, J. *Advanced Organic Chemistry. Reactions, Mechanisms and Structures*, 4th ed.; Wiley: New York, Chichester, Brisbane, Toronto, Singapore, 1992.

(46) Hansch, C.; Leo, A.; Taft, R. W. *Chem. Rev.* **1991**, *91*, 165−195.

(47) (a) Taft, R. W.; Price, E.; Fox, I. R.; Lewis, I. C.; Andersen, K. K.; Davies, G. T. *J. Am. Chem. Soc.* **1963**, *85*, 709−724. (b) Taft, R. W.; Price, E.; Fox, I. R.; Lewis, I. C.; Andersen, K. K.; Davies, G. T. *J. Am. Chem. Soc.* **1963**, *85*, 3146−3156.

(48) Sato, M.; Shintate, H.; Kawata, Y.; Sekino, M.; Katada, M.; Kawata, S. *Organometallics* **1994**, *13*, 1956−1962.

(49) McGrady, J. E.; Lovell, T.; Stranger, R.; Humphrey, M. G. *Organometallics* **1997**, *16*, 4004−4011.

(50) $\Delta E_{\pi,M\to L}$ terms are identified with back-bonding which corresponds to a net electron transfer from occupied metallic orbitals toward the empty π^* orbitals of the alkynyl ligand, in contrast to forward-bonding $\Delta E_{\pi,L\to M}$ terms, which correspond to the transfer of electronic density from the filled π-MO of the acetylide fragment to empty MOs of the metallic fragment.[17c,49]

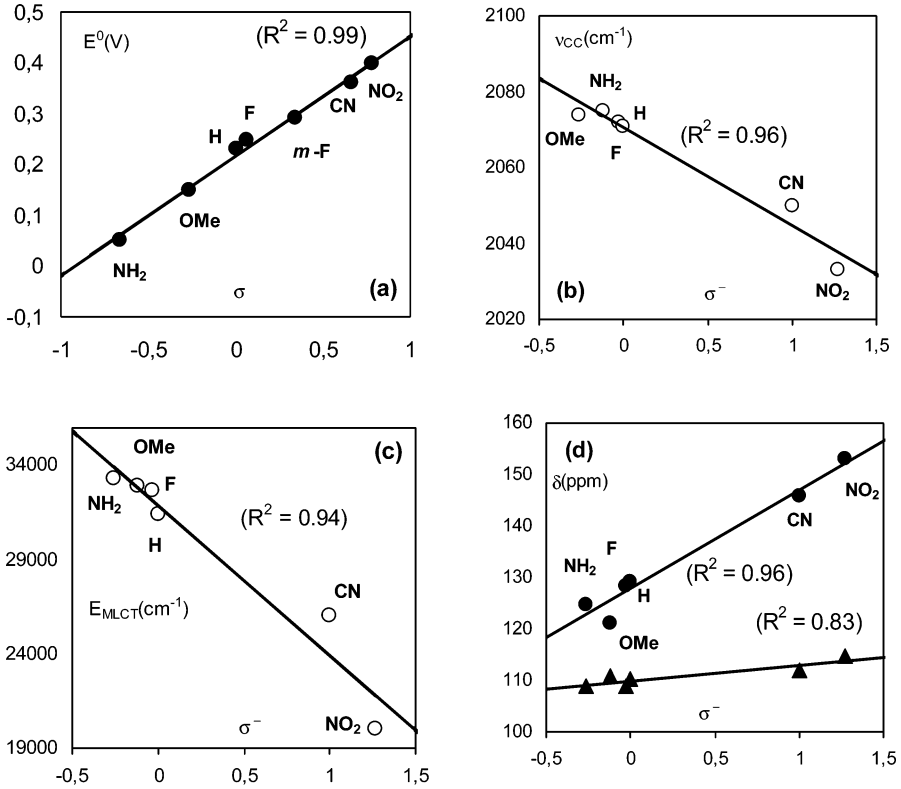

Figure 8. Plots of (a) the Ru(III)/Ru(II) oxidation potentials (V) vs Hammett ESPs (σ) in CH_2Cl_2, (b) the $\nu_{C\equiv C}$ (cm^{-1}) values recorded in CH_2Cl_2, (c) the MLCT energies (cm^{-1}) in CH_2Cl_2, and (d) the alkynyl ^{13}C NMR shifts (ppm) in $CDCl_3$ of the C_α (●) or C_β (▲) vs σ^- ESPs for (η^2-dppe)(η^5-C_5Me_5)Ru(C≡C-1,4-C_6H_4-X) complexes (X = NO_2, CN, F, H, OMe, NH_2).

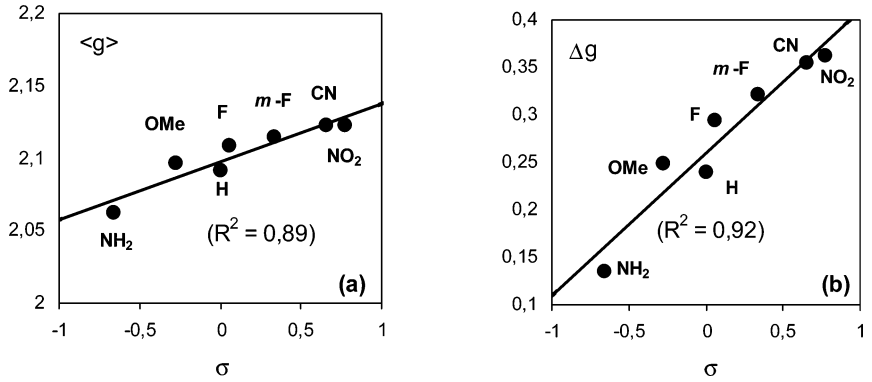

Figure 9. Plots of (a) the ESR mean g value and (b) the **g**-tensor anisotropy vs Hammett ESPs for the complexes [(η^2-dppe)(η^5-C_5Me_5)-Ru(C≡C)-1,4-(C_6H_4)X][PF_6] (X = NO_2, CN, F, H, OMe, NH_2) and [(η^2-dppe)(η^5-C_5Me_5)Ru(C≡C)-1,3-(C_6H_4)F][PF_6].

Apparently, the less favorable energy match between the filled d MOs of the Ru(II) fragment and the empty π^* MOs of the acetylide fragment which should result from the increased ruthenium electronegativity is compensated by a better overlap between these MOs, owing to the larger spatial extension (and better polarizability) of the Ru-based MOs, in line with the improvement of the Pauli term (ΔE_{Pauli}) in the decomposition analysis.[51]

Despite the apparent similarities between MOs of **1a**-H/**1d**-H/**1f**-H and **2a**-H/**2d**-H/**2f**-H, the HOMO−LUMO gap is significantly larger for the Ru(II) complexes (Figure 10). The blue shift observed for the electronic MLCT transition (Figure 6) detected in the UV−visible range for **1a**−**f** is consistent with this observation. The lower lying HOMO for Ru(II) complexes is also certainly at the origin of another notable difference between the two families of complexes, which resides in their oxidation potentials. Indeed, as shown in Figure 1 for the two nitro-substituted complexes, the Ru(II)/Ru(III) oxidation is more difficult by ca. 350 mV for a given substituent with respect to that in the iron(II) analogues.[17a] In apparent conflict with the higher lying LUMO of **1a**-H relative to the Fe(II) analogue **2a**-H, the nitro-centered reduction of **1a** is slightly easier (−1.25 V) than for the Fe(II) analogue **2a** (−1.28 V).[17a] This suggests a slightly lower electron-releasing capability for the Ru(II) center relative to the Fe(II) center, which also contrasts somewhat with the ESP derived for the "(η^2-dppe)(η^5-C_5Me_5)M−C≡C−" fragments (M = Fe, Ru). Indeed, according to the σ values found, the Ru(II)-containing fragment should be slightly more electron-releasing than the Fe(II) one ($\sigma_p = -0.47$ for Ru(II) vs $\sigma_p = -0.37$ for Fe(II)).[24] However, our data also tell us that if the Ru(II)-containing fragment is a comparatively better σ-donor than the Fe(II)-containing one ($\sigma_I = -0.33$ for Ru(II) vs −0.20 for Fe(II)), it has a slightly poorer π-donor ability

(51) The Pauli term in the Fe−C bond is mostly due to repulsive interaction between the filled π-orbitals of the acetylide and the filled π-type orbitals (with strong d character) of the metallic fragment.[17c,49]

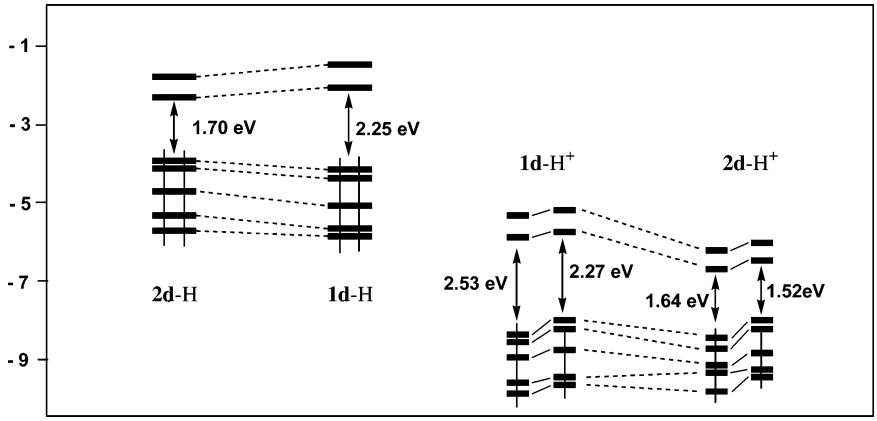

Figure 10. Comparison of the energies (eV) of the frontier MOs of the model complexes $[(H_3P)_2(\eta^5\text{-}C_5H_5)Ru(C{\equiv}CC_6H_5)]^{n+}$ (n = 0, 1; **1d**-H/**1d**-H$^+$) and the corresponding $[(H_3P)_2(\eta^5\text{-}C_5H_5)Fe(C{\equiv}CC_6H_5)]^{n+}$ analogues (n = 0, 1; **2d**-H/**2d**-H$^+$).

Chart 3

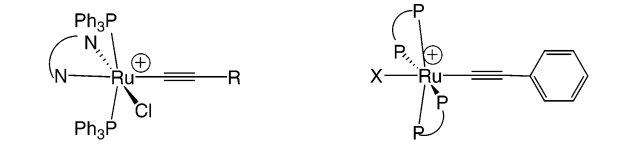

(R = ^{t}Bu, Tol, Ph; N-N = Me_2Bipy) **7a-c**$^+$

(X = CC-Ph, CC-1,4-C_6H_4-CC-Ph, ; P-P = dppe) **8a-b**$^+$

(σ_R = −0.09 for Ru(II) vs −0.12 for Fe(II)).[24] This lower π-donor capability can presently explain the ordering found for the potentials of the nitro-centered reduction, especially if large electronic relaxation comes in play.

Ru(III) Complexes. Oxidation of the Ru(II) complexes yields the corresponding Ru(III) radicals, which proved to be quite reactive species in comparison to the isolable Fe(III) analogues. Again, the DFT computations reveal that the most striking differences reside in a larger delocalization of the unpaired electron on the functional arylacetylide ligand and a larger SOMO−LUMO gap (Figure 10), but the bonding scheme remains rather close to that obtained for the Fe(III) radicals.[9b,17d,52] Mononuclear Ru(III) acetylide radicals being scarce species,[35−36,39,53] we have attempted to gain further insight into their bonding by spectroscopy.

Thus, rhombic ESR signatures with $g_3 > g_2 > g_e > g_1$ (where g_e stands for the free-electron value), were observed for the oxidized Ru(III) complexes which are reminiscent of those obtained for the Fe(III) analogues.[17d] It turns out that the anisotropy found for **1a**−**f**[PF_6] is slightly less than that recently reported by Adams et al. for the Ru(III) acetylide radical cations **7a**−**c**$^+$ (Chart 3).[35,53] We have previously shown for the Fe(III) analogues **2a**−**f**[PF_6] that the anisotropy (Δg) of the signal is related to the extent of delocalization of the unpaired electron on the arylalkynyl ligand.[17d] According to this work, the largest diagonal value of the **g** tensor (g_{zz}), which roughly corresponds to g_3 for **1a**−**f**[PF_6], should be given by eq 6.[54] Considering

$$g_{zz} = g_e + 2\zeta(c_0c_1)^2/\Delta_1 \qquad (6)$$

that the spin−orbit coupling for the Ru(III) center (ζ = 1250 cm^{-1}) is much larger than that for the Fe(III) center (ζ = 460 cm^{-1})[55] for a comparable Δ_1 value (DFT diagrams actually give a comparable SOMO/SOMO − 1 gap within 0.05 eV), we should observe a much larger g_3 (respectively Δg) value. Actually, this is not the case, and a significantly smaller value is obtained for g_3 (respectively Δg) in Ru(III) compounds. This can only be reconciled with eq 6 by considering a much more delocalized unpaired electron (i.e. lower c_0 value) in **1a**−**f**[PF_6], a trend also shown by the DFT computations (Table 12).

The oxidized species **1a**−**f**$^+$ could also be characterized by infrared spectroscopy. A transient absorption located at ca. 1940 cm^{-1} was detected each time, concomitant with the disappearance of the characteristic ν(C≡C) band of the starting Ru(II) precursor. This absorption is typically in the range found for other ν(C≡C) values of mononuclear Ru(III) acetylide complexes such as **7a**−**c**$^+$.[35] Notably, while a decrease in the ν(C≡C) energy is expected upon oxidation (Table 1), the shift was less than that observed with dinuclear butadiynediyl ruthenium complexes.[16a,b,56] However, depending on the substituent, this shift is larger (ca. 140 cm^{-1} for **1a**$^+$ to 35 cm^{-1} for **1e**$^+$) than for the corresponding Fe(III) analogues **2a**−**f**[PF_6].[17a] This suggests a greater bond weakening of the triple bond in the phenylacetylide spacer for **1a**−**f**$^+$ than for **2a**−**f**$^+$, in line with the enhanced delocalization of the unpaired electron in **1a**-H/**1f**-H$^+$ relative to **2a**-H/**2f**-H$^+$ found by DFT calculations.

Finally, our attempts to characterize **1a**−**f**$^+$ by electronic spectroscopy revealed a transient absorption of very weak intensity in the near-IR domain. Electronic transitions in the same spectral range were recently reported by Humphrey and co-workers for the related Ru(III) acetylide complexes **8a**,**b**$^+$ (Chart 3).[13a] These transitions were, however, much more intense than for **1a**−**e**[OTf] and were accordingly assigned to LMCT processes. Much more related to the low-energy transition of **1a**−**f**$^+$ is certainly the electronic absorption detected in the near-IR range for the Fe(III) analogues, which was assigned to a Laporte-forbidden (d−d) SOMO − 2/SOMO transition.[17d] By comparison, this transition would now have experienced a sizable blue shift (ca. 1800−2300 cm^{-1}), a trend that can be roughly retrieved in the SOMO/SOMO − 2 differences in the MO diagrams in the case of the NO_2- and NH_2-substituted complexes, but not between **1d**-H$^+$ and **2d**-H$^+$. Such a discrep-

(52) Connelly, N. G.; Gamasa, M. P.; Gimeno, J.; Lapinte, C.; Lastra, E.; Maher, J. P.; Le Narvor, N.; Rieger, A. L.; Rieger, P. H. *J. Chem. Soc., Dalton Trans.* **1993**, 2575−2578.

(53) Adams, C. J.; Boven, L. E.; Humphrey, M. G.; Morrall, J. P. L.; Samoc, M.; Yellowlees, L. J. *Dalton Trans.* **2004**, 4130−4138.

(54) In these equations, g_e stands for the free-electron g value, c_n values are the coefficients of the d AOs in the frontier MOs, and Δ_1 is the SOMO − 1/SOMO transition energy.

(55) Dunn, T. M. *Trans. Faraday Soc.* **1961**, *57*, 1441−1444.

(56) (a) Bruce, M. I.; Low, P. J.; Costuas, K.; Halet, J.-F.; Best, S. P.; Heath, G. H. *J. Am. Chem. Soc.* **2000**, *122*, 1949−1962. (b) Bruce, M. I.; Denisovich, L. I.; Low, P. J.; Peregudova, S. M.; Ustynyuk, N. A. *J. Chem. Soc., Mendeleev Commun.* **1996**, 200−201.

ancy is not surprising, since open-shell compounds often show large electronic relaxation energies, not apparent in the MO diagrams.

Thus, despite the apparent similarity between the Ru(III) radical species **1a**−**f**$^+$ and the known Fe(III) analogues **2a**−**f**$^+$, the experimental data and DFT calculations point to a larger delocalization of the unpaired electron in the former species. This improved delocalization translates to a sizable radical character not only on the β-carbon atom in these Ru(III) complexes but also on the aryl ring (and even on the X substituent for most electron-releasing groups). It explains the comparably higher reactivity of the Ru(III) complexes, as well as the elusiveness of **1f**$^+$. It also rationalizes (see Table 12) the formation of the vinylidene complex **6**[OTf] in the case of **1a**$^+$, which possibly results from hydrogen abstraction from the solvent. The instability of **1a**−**f**$^+$ radicals, presumably of kinetic origin, has ample precedence with mononuclear Ru(III) acetylides.[35,36] Finally, it is worth mentioning that the cathodic peak potential corresponding to the oxidation of the amino group is slightly lower (0.59 V) than that of the Fe(III) analogue (0.68 V). This tends to indicate that the cationic "[(η^2-dppe)(η^5-C_5Me_5)Ru−C≡C-]$^+$" fragment is slightly more electron-releasing than the "[(η^2-dppe)(η^5-C_5Me_5)Fe−C≡C-]$^+$" fragment.

Substituent Effect and Valence Bond Scheme. When studying the substituent effect with (η^2-dppe)(η^5-C_5Me_5)Fe-(C≡C)-1,4-(C_6H_4)X, we had previously evidenced linear correlations between CV data or between characteristic spectroscopic data and various ESP sets. Likewise here, similar correlations were sought and observed (Figures 8 and 9). The various correlations obtained for the Ru(II/III) complexes **1a**−**f**/**1a**−**f**$^+$ confirm the sizable electronic influence exerted by the X substituent in both redox states, an effect also indicated by DFT computations.[41] Again, a very good linear correlation between redox potential and Hammett ESPs was observed. The recent work of Hurst et al.[57] along with ours on **2a**−**f**/**2a**−**f**$^+$ [17c] seems to indicate that this might be a general feature of redox-active electron-rich acetylide complexes. Relative to the iron analogues **2a**−**f**/**2a**−**f**$^+$, the slope is more pronounced for **1a**−**f**/**1a**−**f**$^+$, evidencing a slightly stronger substituent effect on the metal-centered M(II)/M(III) oxidation potential in the case of ruthenium.

Similarly to the Fe(II) analogues, the Ru(II) complexes also have linear correlations between σ^- ESP and ν(C≡C), the energy of the lowest electronic transition (MLCT) and the ^{13}C acetylide shifts. While this was expected, given the very similar bonding along the "M^{II}−C≡C-1,4-(C_6H_4)X" core, the quite similar slopes found for the regression lines in these correlations were more surprising to us (see Supporting Information). These similarities suggest that changes in composition and energy of the frontier MOs induced by the replacement of the Ru(II) atom by an Fe(II) atom in such compounds do not markedly affect the transmission of the electronic (inductive/mesomeric) effects affecting these spectroscopic signatures. This is certainly because these signatures mostly originate from atoms or functional groups on the arylacetylide ligand, close to the substituent and therefore less dependent on the nature of the metal center. Considering a valence bond (VB) description (Scheme 4) similar to that previously proposed to rationalize the substituent effects for Fe(II) complexes **2a**−**f**,[17c] ν(C≡C), the energy of the lowest electronic transition (MLCT), and the ^{13}C acetylide shifts point, however, to a slightly lower weight of the cumulenic VB mesomers (B/D) in the ground state (GS) of Ru(II) complexes

Scheme 4

Moderate to Strong

Electron-releasing X Substituents

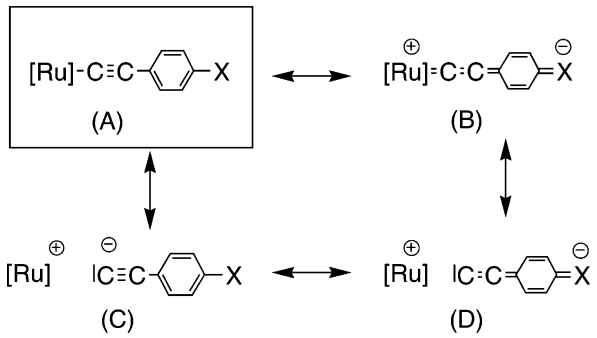

Strongly Electron-withdrawing

X Substituents

Scheme 5

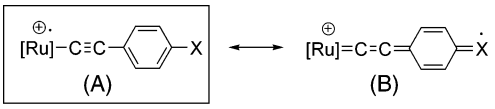

Strongly electron-withdrawing X substituents

1a−**f**. This makes sense, considering the lower hyperpolarizabilities $(\beta_0)_{EFISH}$ found for **1a**,**b** relative to those for the corresponding iron analogues.[12]

The situation is slightly different for the Ru(III) derivatives, where larger differences in bonding have been established by DFT calculations, essentially in terms of electronic delocalization. Here, no significant correlation with ν(C≡C) could be obtained, in contrast to Fe(III) derivatives,[17b] but a significant correlation with ESR data was found. These fits were poorer than those obtained with Fe(III) analogues and were obtained with σ ESPs rather than with σ^+ ESPs, suggesting a stronger inductive influence of the substituent in **1a**−**f**$^+$ than in **2a**−**f**$^+$. Presently, on the basis of a perturbational approach of ESR shifts,[17d,39,58] this stronger inductive influence might be traced back to the larger spread on the functional arylacetylide ligand of the higher lying spin orbitals having a sizable metal character along with a sizable σ-character, and particularly in the SOMO − 2 among the frontier MOs (Figure 7).[59] The larger slopes found for the regression lines (eqs 5a,b) can easily be understood as due to the larger spin−orbit coupling parameter operative for Ru(III) relative to Fe(III) metal centers. Owing to the strong similarities between **1a**−**f**$^+$ and **2a**−**f**$^+$ suggested by the spectroscopic data, we also propose a VB scheme similar to that previously advanced for the Fe(III) derivatives to rationalize the substituent effects in **1a**−**f**$^+$ in the GS (Scheme 5).

Conclusion

We have reported here the isolation and characterization of several electron-rich Ru(II) acetylide complexes of the formula

(57) Hurst, S. K.; Xu, G.-L.; Ren, T. *Organometallics* **2003**, *22*, 4118−4123.

(58) Rieger, A. L.; Rieger, P. H. *Organometallics* **2004**, *23*, 154−162.

(59) Schilling, B. E. R.; Hoffmann, R.; Lichtenberger, D. L. *J. Am. Chem. Soc.* **1979**, *101*, 585−591.

(η^2-dppe)(η^5-C_5Me_5)Ru(C≡C)-1,4-(C_6H_4)X (**1a**−**f**) and also the in situ characterization of the corresponding Ru(III) congeners (**1a**−**f**$^+$). In contrast to the known Fe(III) analogues (**2a**−**f**/**2a**−**f**$^+$), these radical cations proved to be too reactive to be isolated. DFT computations on [$(H_3P)_2$(η^5-C_5H_5)Ru(C≡C)-1,4-(C_6H_4)X]$^{0/+}$ model complexes along with available experimental data on **1a**−**f**/**1a**−**f**$^+$ indicate that, despite presenting very close electronic structures to those of the known iron analogues, the frontier MOs are slightly more weighted on the acetylide spacer in the case of ruthenium. This leads to a stronger delocalization of the unpaired electron on the arylacetylide ligand in Ru(III) complexes and explains their enhanced reactivity. Very good correlations between oxidation potentials or selected infrared, UV, or NMR spectral data and various ESP sets were obtained for the Ru(II) complexes, while good linear correlations with the ESR rhombic *g* tensors were found with Ru(III) derivatives, which overall confirm a comparable or slightly improved electronic communication between the functional aryl group and the metal center in comparison to the iron analogues in both redox states. Finally, we also showed that the magnitude of the $d_M-\pi^*_{C\equiv C}$ back-donation is quite unaffected when ruthenium replaces iron in these M(II) acetylide complexes.

Experimental Section

General Data. All manipulations were carried out under an inert atmosphere. Solvents or reagents were used as follows: Et_2O and *n*-pentane, distilled from Na/benzophenone; CH_2Cl_2, distilled from CaH_2 and purged with argon; $HNPr^i_2$, distilled from KOH and purged with argon; aryl bromides (Acros, >99%), opened/stored under Ar. High-field NMR spectra experiments were performed on a multinuclear Bruker 300 or 200 MHz instrument (AM300WB and 200DPX). Chemical shifts are given in parts per million relative to tetramethylsilane (TMS) for ^{1}H and ^{13}C NMR spectra and external H_3PO_4 for ^{31}P NMR spectra. Transmittance FTIR spectra were recorded using a Bruker IFS28 spectrometer (400−4000 cm^{-1}). Raman spectra of the solid samples were obtained by diffuse scattering on the same apparatus and recorded in the 100−3300 cm^{-1} range (Stokes emission) with a laser excitation source at 1064 nm, using a 1.05−1.06 μm laser source (15 mW) and a quartz separator with a FRA 106 detector. Liquid near-IR spectra were recorded on Cary 5 and JASCO V-570 spectrometers. UV−visible spectra were recorded on an UVIKON 942 spectrometer. Cyclic voltammograms were recorded using a PAR 263 instrument in CH_2Cl_2 (0.1 M [NBu_4][PF_6]) at 25 °C at a platinum electrode, using a SCE reference electrode and ferrocene as internal calibrant (0.460 V).[33] EPR spectra were recorded on a Bruker EMX-8/2.7 (X-band) spectrometer. LSI/ESI-MS analyses were carried out at the "Centre Regional de Mesures Physiques de l'Ouest" (CRMPO, Rennes, France) on a high-resolution MS/MS ZabSpec TOF Micromass spectrometer (8 kV). Elemental analyses were performed at the Centre for Microanalyses of the CNRS at Lyon-Solaise, France, at the CRMPO.

The complexes (η^5-C_5Me_5)(η^2-dppe)RuCl (**3**) and (η^5-C_5Me_5)-(η^2-dppe)Ru(C≡CH) (**4**)[60] as well as the functionalized alkynes RC≡C-1,4-(C_6H_4)X (R = $SiMe_3$, H; X = NO_2, CN, F, H, OMe, NH_2)[61] were synthesized by reported procedures. Other compounds were commercially available and were used as such.

(η^2-dppe)(η^5-C_5Me_5)Ru(C≡C)-1,4-(C_6H_4)NO_2 (1a). Method A, via Alkyne Activation. The orange chloro precursor complex (η^5-C_5Me_5)(η^2-dppe)RuCl (**3**; 0.200 g, 0.29 mmol), [NBu_4][PF_6] (0.005 g, 0.46 mmol), and $Me_3SiC\equiv C(C_6H_4NO_2)$-4 (0.100 g, 0.45 mmol) were introduced under argon in a Schlenk flask. Subsequently, 15 mL of methanol were added and the mixture was refluxed for 20 h. The solvent was evacuated, and the orange residue was analyzed (infrared and NMR) to check the complete conversion into the corresponding vinylidene (^{31}P{^{1}H} NMR (δ, $CDCl_3$, 200 MHz): 72.3 (s, dppe); 143.1 (septuplet, $^1J_{PF}$ = 712 Hz, PF_6^-)). Then, potassium *tert*-butoxide (0.050 g, 0.45 mmol) and 15 mL of methanol were introduced and the reaction medium was stirred for 12 h at ambient temperature. The desired alkynyl complex (η^2-dppe)(η^5-C_5Me_5)Ru(C≡C)-1,4-(C_6H_4)NO_2 (**1a**) precipitated as a purple powder, which was filtered on a frit, washed with methanol (3 × 5 mL), and dried in vacuo. Yield: 0.180 g (80%).

Method B, via Catalytic Sonogashira Coupling. The orange complex (η^5-C_5Me_5)(η^2-dppe)Ru(C≡CH) (**4;** 0.100 g, 0.15 mmol), the $(PPh_3)_2PdCl_2$ catalyst precursor (0.005 g, ca. 5%), and CuI cocatalyst (0.003 g, ca. 10%) were introduced in a Schlenk flask under argon. Subsequently *p*-$BrC_6H_4NO_2$ (0.091 g, 0.45 mmol) was added into 10 mL of $HNPr^i_2$ and the mixture was refluxed for 12 h. The solvent was cryogenically trapped, and the dark residue was extracted with toluene and the extract filtered on a Celite pad. The extract is a mixture of the desired complex (ca. 80% by ^{1}H NMR) and *p*-$BrC_6H_4NO_2$. Evaporation of the toluene and elution through a neutral alumina column using an *n*-pentane/diethyl ether gradient, followed by repeated methanol washings (3 × 10 mL), allowed isolation of the desired complex (η^2-dppe)(η^5-C_5Me_5)Ru(C≡C)-1,4-(C_6H_4)NO_2 (**1a**) as a purple powder in a pure state, albeit with a lower yield (0.055 g, ca. 20%) after drying in vacuo. Anal. Calcd for $C_{44}H_{43}NO_2P_2Ru$: C, 67.68; H, 5.55; N. 1.79. Found: C, 67.24; H, 5.71; N. 1.88. MS (positive LSI, 3-NBA, *m*/*z*): 781 ([**1a**]$^+$, 90%); 635 ([(dppe)(C_5Me_5)Ru]$^+$, 100%). FT-IR (ν, KBr, cm^{-1}): 2050 (vs, C≡C); 2014 (m, C≡C); 1577, 1320 (vs, NO_2). Raman (ν, cm^{-1}) 2046 (m, C≡C); 2011 (w, C≡C); 1578 (m, NO_2); 1322 (vs, NO_2). ^{31}P NMR (δ, $CDCl_3$, 81 MHz): 81.7 (s, 2P, dppe). ^{1}H NMR (δ, $CDCl_3$, 200 MHz): 7.90 (d, 2H, $^3J_{HH}$ = 9.0 Hz, $H_{ortho/ArNO_2}$); 7.69 (m, 4H, $H_{ortho/Ar/dppe}$); 7.37−7.19 (m, 16H, $H_{Ar/dppe}$); 6.67 (d, 2H, $^3J_{HH}$ = 9.0 Hz, $H_{meta/ArNO2}$); 2.65 (m, 2H, CH_{2dppe}); 2.11 (m, 2H, CH_{2dppe}); 1.58 (s, 15H, $C_5(CH_3)_5$). ^{13}C{^{1}H} NMR (δ, $CDCl_3$, 75 MHz): 153.0 (t, $^2J_{CP}$ = 25 Hz, Ru−*C*≡C); 142.5 (s, C_{quat}); 138.8 (s, C_{quat}); 138.8−127.7 (m, 8$C_{Ar/dppe}$ + *C*−H_{ArNO_2}); 123.9 (s, *C*−H_{ArNO_2}); 114.6 (s, $^2J_{CH}$ = 4.4 Hz, C_{quat}); 93.7 (s, $C_5(CH_3)_5$); 29.9 (m, $CH_{2,dppe}$); 10.4 (s, $C_5(CH_3)_5$).

Crystals of **1a** were grown by slow diffusion of methanol into a chloroform solution of **1a** (layer/layer).

(η^2-dppe)(η^5-C_5Me_5)Ru(C≡C)-1,4-(C_6H_4)CN (1b). Complex **1b** was isolated by following method B as a yellow solid from the complex (η^5-C_5Me_5)(η^2-dppe)Ru(C≡CH) (**3**) and *p*-BrC_6H_4CN. Yield: 88%. Anal. Calcd for $C_{45}H_{43}NP_2Ru$: C, 71.04; H, 5.70; N, 1.84. Found: C, 70.03; H, 5.69; N, 1.82. MS (positive LSI, 3-NBA, *m*/*z*): 761 ([**1b**,H]$^+$, 95%); 635 ([(dppe)(C_5Me_5)Ru]$^+$, 100%). FT-IR (ν, KBr, cm^{-1}): 2286 (m, C≡N); 2071 (sh, C≡C); 2059 (vs, C≡C); 2034 (m, C≡C). Raman (ν, cm^{-1}): 2219 (m, C≡N); 2074 (vs, C≡C); 2060 (sh, C≡C); 2048 (sh, C≡C). ^{31}P NMR (δ, $CDCl_3$, 81 MHz): 81.8 (s, 2P, dppe). ^{1}H NMR (δ, $CDCl_3$, 200 MHz): 7.71 (m, 4H, $H_{ortho/Ar/dppe}$); 7.36−7.24 (m, 18H, $H_{Ar/dppe}$ + $H_{ortho/ArCN}$); 6.69 (d, $^2J_{HH}$ = 8.4 Hz, 2H, $H_{meta/ArCN}$); 2.63 (m, 2H, $CH_{2,dppe}$); 2.07 (m, 2H, $CH_{2,dppe}$); 1.57 (s, 15H, $C_5(CH_3)_5$). ^{13}C{^{1}H} NMR (δ, $CDCl_3$, 75 MHz): 145.7 (t, $^2J_{CP}$ = 24 Hz, Ru−*C*≡C); 136.2 (s, C_{quat}); 139.2−127.4 (m, 8$C_{Ar/dppe}$ + 2*C*-H_{ArCN} + $C_{quat/ArCN}$); 121.1 (s, *Ar*−*C*N); 112.0 (s, C_{quat}); 104.4 (s, C_{quat}); 93.6 (s, $C_5(CH_3)_5$); 29.8 (m, CH_{2dppe}); 10.5 (s, $C_5(CH_3)_5$).

Crystals could be grown by slow evaporation of a benzene solution of **1b**.

(η^2-dppe)(η^5-C_5Me_5)Ru(C≡C)-1,4-(C_6H_4)F (1c). Complex **1c** was isolated by following method B as a yellow solid from the complex (η^5-C_5Me_5)(η^2-dppe)Ru(C≡CH) (**3**) and *p*-BrC_6H_4F. Yield: 77%. Anal. Calcd for $C_{44}H_{43}FP_2Ru$: C, 70.11; H, 5.75.

(60) Bruce, M. I.; Ellis, B. G.; Gaudio, M.; Lapinte, C.; Melino, G.; Paul, F.; Skelton, B. W.; Smith, M. E.; Toupet, L.; White, A. H. *Dalton Trans.* **2004**, 1601−1609.

(61) Lavastre, O.; Ollivier, L.; Dixneuf, P. H.; Sinbandhit, S. *Tetrahedron* **1995**, *52*, 5495−5504.

Found: C, 70.14; H, 5.80. MS (positive LSI, 3-NBA, *m*/*z*): 754 ([**1c**]$^+$, 50%); 635 ([(dppe)(C_5Me_5)Ru]$^+$, 10%). FT-IR (ν, KBr, cm^{-1}): 2086 (s, C≡C). Raman (ν, neat, cm^{-1}): 2085 (s, C≡C). ^{31}P NMR (δ, $CDCl_3$, 81 MHz): 82.1 (s, 2P, dppe). ^{19}F{^{1}H} NMR (δ, $CDCl_3$, 188 MHz, ppm): −120.3 (s, C_6H_4F). ^{1}H NMR (δ, $CDCl_3$, 200 MHz): 7.82 (m, 4H, $H_{ortho/dppe}$); 7.60−7.20 (m, 16H, $H_{Ar/dppe}$); 6.72 (d, 4H, H_{ArF}); 2.68 (m, 2H, $CH_{2,dppe}$); 2.07 (m, 2H, $CH_{2,dppe}$); 1.57 (s, 15H, $C_5(CH_3)_5$). ^{13}C{^{1}H} NMR (δ, $CDCl_3$, 125 MHz, ppm): 160.0 (d, $^1J_{CF}$ = 241 Hz, F−C_{ArF}); 128.3 (t, $^2J_{CP}$ = 25 Hz, Fe−C≡C); 139.8−127.8 (m, 8$C_{Ar/dppe}$ + $C_{quat/ArF}$); 131.9 (d, $^2J_{CF}$ = 7 Hz, C−$H_{meta/ArF}$); 114.9 (d, $^2J_{CF}$ = 21 Hz, C−$H_{ortho/ArF}$); 108.9 (s, Fe−C≡C); 93.2 (s, $C_5(CH_3)_5$); 30.1 (m, $CH_{2,dppe}$); 10.8 (s, $C_5(CH_3)_5$).

Crystals could be grown by layering a dichloromethane solution of **1c** with *n*-pentane.

(η^2-dppe)(η^5-C_5Me_5)Ru(C≡C)-1,3-(C_6H_4)F (1c-*m*). Complex **1c**-*m* was isolated by following method B as a yellow solid from the complex (η^5-C_5Me_5)(η^2-dppe)Ru(C≡CH) (**3**) and *m*-BrC_6H_4F. Yield: 70%. Anal. Calcd for $C_{44}H_{43}FP_2Ru$: C, 70.11; H, 5.75. Found: C, 69.98; H, 5.71. MS (positive LSI, 3-NBA): *m*/*z* 754 ([**1c**-*m*]$^+$, 45%); 635 ([(dppe)(C_5Me_5)Ru]$^+$, 15%). FT-IR (ν, KBr, cm^{-1}): 2070, 2057 (vs, C≡C). Raman (ν, neat, cm^{-1}): 2060 (s, C≡C). ^{31}P NMR (δ, $CDCl_3$, 81 MHz): 82.0 (s, 2P, dppe). ^{19}F{^{1}H} NMR (δ, $CDCl_3$, 188 MHz, ppm): −116.3 (s, C_6H_4F). ^{1}H NMR (δ, $CDCl_3$, 200 MHz): 7.76 (m, 4H, $H_{ortho/dppe}$); 7.60−7.20 (m, 16H, $H_{Ar/dppe}$); 7.00−6.30 (m, 4H, H_{ArF}); 2.68 (m, 2H, $CH_{2,dppe}$); 2.09 (m, 2H, $CH_{2,dppe}$); 1.57 (s, 15H, $C_5(CH_3)_5$). ^{13}C{^{1}H} NMR (δ, $CDCl_3$, 125 MHz, ppm): 163.3 (d, $^1J_{CF}$ = 243 Hz, F−C_{Ar}); 133.5 (t, $^2J_{CP}$ = 25 Hz, Fe−C≡C); 129.2 (d, $^3J_{CF}$ = ca. 10 Hz, C≡CC_{ArF}); 139.8−128.0 (m, 8$C_{Ar/dppe}$); 129.2 (d, $^3J_{CF}$ = ca. 9 Hz, C−H_{ArF}); 126.6 (s,$^4J_{CF}$ < 2 Hz, C−H_{ArF}); 117.2 (d, $^2J_{CF}$ = ca. 20 Hz, $^1J_{CH}$ = 163 Hz, C−H_{ArF}); 109.8 (d, $^2J_{CF}$ = ca. 21 Hz, $^1J_{CH}$ = 164 Hz, C−H_{ArF}); 109.8 (s, Fe−C≡C, $^4J_{CF}$ = ca. 3 Hz); 93.3 (s, $C_5(CH_3)_5$); 30.4 (m, $CH_{2,dppe}$); 10.7 (s, $C_5(CH_3)_5$).

Crystals could be grown by layering a dichloromethane solution of **1c**-*m* with *n*-pentane.

(η^2-dppe)(η^5-C_5Me_5)Ru(C≡C−C_6H_5) (1d). This complex was prepared as previously described.[16c,20] Anal. Calcd for $C_{44}H_{44}P_2Ru$: C, 71.82; H, 6.03. Found: C, 71.66; H, 5.88. MS (positive ESI, CH_2Cl_2, *m*/*z*): 737 ([**1d**,H]$^+$, 85%); 663 ([(dppe)(C_5Me_5)RuCO]$^+$, 90%); 635 ([(dppe)(C_5Me_5)Ru]$^+$, 100%). FT-IR (ν, KBr, cm^{-1}): 2068 (vs, C≡C). Raman (ν, cm^{-1}): 2066 (s, C≡C). ^{31}P NMR (δ, $CDCl_3$, 81 MHz): 82.3 (s, 2P, dppe). ^{1}H NMR (δ, $CDCl_3$, 200 MHz): 7.96 (m, 4H, $H_{ortho/Ar/dppe}$); 7.60−6.90 (m, 21H, $H_{Ar/dppe}$ + H_{Ph}); 2.85 (m, 2H, $CH_{2,dppe}$); 2.22 (m, 2H, $CH_{2,dppe}$); 1.74 (s, 15H, $C_5(CH_3)_5$). ^{13}C{^{1}H} NMR (δ, $CDCl_3$, 50 MHz): 129.3 (t, $^2J_{CP}$ = 25 Hz, Ru−C≡C); 131.7 (s, CC≡C); 139.8−127.2 (m, 8$C_{Ar/dppe}$ + 2C−H_{Ph}); 122.9 (s, $^1J_{CH}$ = 161 Hz, C−H_{Ph}); 110.2 (s, $^3J_{CH}$ = 4.5 Hz, Ru−C≡C); 92.9 (s, $C_5(CH_3)_5$); 29.8 (m, $CH_{2,dppe}$); 10.5 (s, $C_5(CH_3)_5$).

Crystals were grown by slow evaporation of a dichloromethane/*n*-pentane (50/50) solution of **1d**.

(η^2-dppe)(η^5-C_5Me_5)Ru(C≡C)-1,4-(C_6H_4)OMe (1e). Complex **1e** was isolated by following method A as a yellow solid from the complex (η^5-C_5Me_5)(η^2-dppe)RuCl (**2**) and HC≡C(C_6H_4OMe)-4. Yield: 68%. Anal. Calcd for $C_{45}H_{46}OP_2Ru$: C, 70.57; H, 6.05. Found: C, 70.50; H, 5.95. MS (positive ESI, CH_2Cl_2, *m*/*z*): 767 ([**1e**,H]$^+$, 65%); 663 ([(dppe)(C_5Me_5)RuCO]$^+$, 100%); 635 ([(dppe)-(C_5Me_5)Ru]$^+$, 90%). FT-IR (ν, KBr, cm^{-1}): 2073 (vs, C≡C). Raman (ν, cm^{-1}): 2075 (s, C≡C). ^{31}P NMR (δ, $CDCl_3$, 81 MHz): 82.3 (s, 2P, dppe). ^{1}H NMR (δ, $CDCl_3$, 200 MHz): 7.86 (m, 4H, $H_{ortho/Ar/dppe}$); 7.60−7.00 (m, 20H, $H_{Ar/dppe}$); 6.78−6.70 (m, 4H, H_{ArOMe}); 3.78 (s, 3H, OCH_3); 2.80 (m, 2H, $CH_{2,dppe}$); 2.15 (m, 2H, $CH_{2,dppe}$); 1.63 (s, 15H, $C_5(CH_3)_5$). ^{13}C{^{1}H} NMR (δ, $CDCl_3$, 50 MHz): 156.0 (s, C_{quat}); 139.8−127.2 (m, 8$C_{Ar/dppe}$ + 2C−H_{ArOMe}); 124.8 (s, CC≡C); 124.6 (t, $^2J_{CP}$ = 25 Hz, Ru−C≡C); 124.1 (s, $^1J_{CH}$ = 158 Hz, C−H_{ArOMe}); 108.8 (s, Ru−C≡C); 92.9 (s, $C_5(CH_3)_5$); 55.7 (s, OCH_3), 29.8 (m, $CH_{2,dppe}$); 10.5 (s, $C_5(CH_3)_5$).

Crystals could be grown by slow evaporation of a dichloromethane solution of **1e**.

(η^2-dppe)(η^5-C_5Me_5)Ru(C≡C)-1,4-(C_6H_4)NH_2 (1f). Complex **1f** was isolated by following method A as an orange solid from the complex (η^5-C_5Me_5)(η^2-dppe)RuCl (**2**) and HC≡C($C_6H_4NH_2$)-4. Yield: 43%. Anal. Calcd for $C_{44}H_{45}NP_2Ru$: C, 70.38; H, 6.04; N, 1.87. Found: C, 70.38; H, 6.05; N, 2.08. MS (positive, ESI, CH_2Cl_2, *m*/*z*): 752 ([**1f**,H]$^+$, 85%); 635 ([(dppe)(C_5Me_5)Ru]$^+$, 40%). FT-IR (ν, KBr, cm^{-1}) 2072 (vs, C≡C). Raman (ν, cm^{-1}): 2074 (s, C≡C). ^{31}P NMR (δ, $CDCl_3$, 81 MHz): 82.3 (s, 2P, dppe). ^{1}H NMR (δ, $CDCl_3$, 200 MHz): 7.82 (m, 4H, $H_{ortho/Ar/dppe}$); 7.50−7.10 (m, 20H, $H_{Ar/dppe}$); 6.67 (d, $^2J_{HH}$ = 7.8 Hz, 2H, H_{ArNH_2}); 6.45 (d, $^2J_{HH}$ = 7.8 Hz, 2H, H_{ArNH_2}); 3.43 (s, 2H, NH_2); 2.75 (m, 2H, $CH_{2,dppe}$); 2.10 (m, 2H, $CH_{2,dppe}$); 1.59 (s, 15H, $C_5(CH_3)_5$). ^{13}C-{^{1}H} NMR (δ, C_6D_6, 50 MHz): 143.7 (s, C_{quat}); 139.8−127.2 (m, 8$C_{Ar/dppe}$ + 2C−H_{ArNH_2}); 123.1 (s, Ru−C≡C); 121.1 (t, $^2J_{CP}$ = 25 Hz, Ru−C≡C); 115.6 (s, C−H_{ArNH_2}); 110.7 (s, CC≡C); 93.2 (s, $C_5(CH_3)_5$); 30.4 (m, $CH_{2,dppe}$); 11.1 (s, $^1J_{CH}$ = 127 Hz, $C_5(CH_3)_5$).

Crystals could be grown by layering a dichloromethane solution of **1f** with *n*-pentane.

Attempted Oxidation of (η^2-dppe)(η^5-C_5Me_5)Ru(C≡C)-1,4-(C_6H_4)NO_2 (1a). A 0.92 equiv portion of AgOTf (0.014 g, 0.054 mmol) was added to a solution of **1a** (0.050 g, 0.059 mmol) in 10 mL of dichloromethane, resulting in a darkening of the solution. Stirring was maintained for 3 h at room temperature, and the solution was concentrated in vacuo to ca. 2 mL. Addition of 10 mL of diethyl ether precipitated a brown-orange solid, after decantation and subsequent washing with 2 × 3 mL portions of toluene followed by 2 × 3 mL of diethyl ether and drying in vacuo. Extraction with 5 mL of dichloromethane, followed by filtration on a Celite plug and evaporation of the solvent, yielded a brown-green solid. The latter proved to be a mixture of several compounds, containing no more starting **1a**. Small red-orange needles were isolated after concentration of the washings to dryness (0.030 g), redissolution in dichloromethane, and slow evaporation of the solvent. The solid-state structure of the compound was solved. The latter proved to be the vinylidene complex [(η^2-dppe)(η^5-C_5Me_5)-Ru(=C=CH)-1,4-(C_6H_4)NO_2][OTf] (**6**[OTf]); relevant parameters are given in the Supporting Information. No other compound could be purified or identified in the resulting mixture.

Infrared and Near-IR Measurements on Ru(III) Complexes. The Ru(II) complexes were dissolved in dichloromethane (ca. 5 × 10^{-3} M), and the spectrum of the Ru(II) sample was recorded for comparison purposes. A slight excess of silver triflate (AgOTf) was next suspended in the solution, and the mixture was sonicated for a few minutes before being transferred to the spectrometer. The spectra were then immediately recorded at 20 °C.

ESR Measurements on Ru(III) Complexes. The Ru(II) complexes were ground with a slight excess of [(η^5-C_5H_5)$_2$Fe][PF_6] and introduced in a ESR tube under an argon-filled atmosphere, a 1:1 mixture of degassed dichloromethane/1,2-dichloroethane was transferred to dissolve the solid, just before being frozen at 77 K, and the tubes were sealed and transferred into the ESR cavity. The spectra were immediately recorded at that temperature.

^{19}F NMR Derivation of Hammett Parameters for "(η^2-dppe)-(η^5-C_5Me_5)Ru−C≡C−". Samples of the compounds **1c** and **1c**-*m* (0.05 mmol) were each dissolved in 1 mL of freshly distilled and degassed CCl_4. These solutions were then transferred into NMR tubes under argon, and 5 μL (0.076 mmol) of fluorobenzene was syringed into the tube, as internal reference. After homogenization of the solution, the ^{19}F{^{1}H} NMR spectra were recorded at 25 °C. The values of σ_I and σ_R were derived from the values of the various ^{19}F NMR shift differences, using the correlations established by Taft and co-workers for *m*- and *p*-fluorobenzene derivatives.[46] From these values, σ_p and σ_m were then computed.

Computational Details. DFT calculations were carried out using the Amsterdam Density Functional (ADF) program.[62−64] The model compounds $[(PH_3)_2(\eta^5\text{-}C_5H_5)Ru(C{\equiv}C)\text{-}1,4\text{-}(C_6H_4)X]^{n+}$ (X = NO_2, H, NH_2; n = 0, 1) were used in order to reduce computational effort. Electron correlation was treated within the local density approximation (LDA) in the Vosko−Wilk−Nusair parameterization.[65] The nonlocal corrections of Becke[66] and of Perdew[67] were added to the exchange and correlation energies, respectively. The numerical integration procedure applied for the calculations was developed by te Velde et al.[62−64] The basis set used for the metal atoms was a triple-ζ Slater-type orbital (STO) basis for Ru 4d and 5s and a single-ζ function for Ru 5p. A triple-ζ STO basis set was employed for H 1s and for 2s and 2p of C, N and O, extended with a single-ζ polarization function (2p for H; 3d for C, N, and O) for X groups. The valence orbitals of the atoms of the other groups (C_5H_5, PH_3) were described by a double-ζ STO basis set. Full geometry optimizations (assuming C_1 symmetry) were carried out on each complex, using the analytical gradient method implemented by Versluis and Ziegler.[68] Spin-unrestricted calculations were performed for all the considered open-shell systems. Decomposition of the Ru−C_α interaction energy was done according to the *transition state* method of Ziegler and Rauk,[42,43] as previously described.[17c] Optimized geometries with C_s symmetry were used. The latter were calculated to be not more than 1 kcal/mol less stable than the systems optimized without symmetry constraints.

Crystallography. Crystals of **1a**−**f** and **1c**-*m* were obtained as described above. The samples were studied on a NONIUS Kappa CCD diffractometer with graphite-monochromatized Mo Kα radiation. The cell parameters were obtained with Denzo and Scalepack with 10 frames (ψ rotation: 1° per frame).[69] The data collection[70] ($2\theta_{max}$, number of frames, Ω rotation, scan rate, and *hkl* ranges are given in Table 1) gave 53 280, 19 532, 50 379, 13 286, 33 478, 38 712, and 33 926 reflections for **1a**−**f** and **1c**-*m*, respectively. Data reduction with Denzo and Scalepack[69] gave the independent reflections (Table 1). The structures were solved with SIR-97, which revealed the non-hydrogen atoms.[71] After anisotropic refinement, the remaining atoms were found in Fourier difference maps. The complete structures were then refined with SHELXL97[72] by the full-matrix least-squares technique (use of F^2 magnitude; x, y, z, β_{ij} for Fe, P, C, N, and/or O atoms, x, y, z in riding mode for H atoms with variables "*N*(var)", observations and "*w*" used as defined in Table 1). Atomic scattering factors were taken from the literature.[73] ORTEP views of **1a**−**f** and **1c**-*m* were realized with PLATON98.[74] All the calculations were performed on a Pentium NT Server computer.

Acknowledgment. These studies were facilitated by travel grants (ARC of Australia, and CNRS of France). F.P., K.C., and J.-F.H. thank the Pôle de Calcul Intensif de l'Ouest (PCIO) of the University of Rennes and the Institut de Développement et de Ressources en Informatique Scientifique (IDRIS-CNRS) for computing facilities.

Supporting Information Available: Figures displaying an ORTEP diagram of **6**[OTf], IR monitoring of the oxidation of **1b, and** UV spectra of **1b**[OTf] and **1e**[OTf], comparative tables of slopes and R^2 indices for the correlations obtained between spectroscopic data for Fe(II) and Ru(II) complexes, tables giving full details of the X-ray structure of **6**[OTf], including tables of atomic positional parameters, bond distances and angles, anisotropic and isotropic thermal displacement parameters, and CIF files giving crystal data for **1a**−**f** and **1c**-***m***. This material is available free of charge via the Internet at http://pubs.acs.org.

OM050799T

(62) te Velde, G.; Bickelhaupt, F. M.; Fonseca Guerra, C.; van Gisbergen, S. J. A.; Baerends, E. J.; Snijders, J.; Ziegler, T. *Theor. Chim. Acc.* **2001**, *22*, 931−967.

(63) Fonseca Guerra, C.; Snijders, J.; te Velde, G.; Baerends, E. J. *Theor. Chim. Acc.* **1998**, *99*, 391−403.

(64) ADF2.3 and ADF2002.01; Theoretical Chemistry, Vrije Universiteit, Amsterdam, The Netherlands, SCM.

(65) Vosko, S. D.; Wilk, L.; Nusair, M. *Can. J. Chem.* **1990**, *58*, 1200−1211.

(66) (a) Becke, A. D. *J. Chem. Phys.* **1986**, *84*, 4524−4529. (b) Becke, A. D. *Phys. Rev. A* **1988**, *38*, 3098−3100.

(67) (a) Perdew, J. P. *Phys. Rev. B* **1986**, *33*, 8822−8824. (b) Perdew, J. P. *Phys. Rev. B* **1986**, *34*, 7406.

(68) Versluis, L.; Ziegler, T. *J. Chem. Phys.* **1988**, *88*, 322−328.

(69) Otwinowski, Z.; Minor, W. In *Methods in Enzymology*; Carter, C. W., Sweet, R. M., Eds.; Academic Press: London, 1997; Vol. 276, pp 307−326.

(70) Nonius, B. V. Kappa CCD Software; Enraf-Nonius, Delft, The Netherlands, 1999.

(71) Altomare, A.; Burla, M. C.; Camalli, M.; Cascarano, G.; Giacovazzo, C.; Guagliardi, A.; Moliterni, A. G. G.; Polidori, G.; Spagna, R. *J. Appl. Chem.* **1998**, *31*, 74−77.

(72) Sheldrick, G. M. SHELX97-2. Program for the Refinement of Crystal Structures; University of Göttingen, Göttingen, Germany, 1997.

(73) Reidel: D. *International Tables for X-ray Crystallography*; Kynoch Press (present distributor D. Reidel, Dordrecht, The Netherlands): Birmingham, U.K., 1974; Vol. IV.

(74) Spek, A. L. PLATON. A Multipurpose Crystallographic Tool; Utrecht University: Utrecht, The Netherlands, 1998.